

# Estimating the Human Health Effects of Urban Heat in LA County

Kaylee Wei

*Mentor: Hannah Druckenmiller*

## Abstract

Since the Industrial Revolution, Earth's global climate has warmed to unprecedented levels, driven largely and unequivocally by anthropogenic activities. This warming has led to wide-ranging consequences, including increased extreme weather events and poorer public health. Extreme heat in particular has become a key concern, due to its large role in public health as well as its prevalence in urban areas due to the urban heat island effect, in which the built environment elevates local temperatures. However, while the temperature increases associated with urban heat islands are comparable to those projected by end-of-century climate change scenarios, the impacts of urban heat have received relatively less attention from the public and policymakers. We aim to address this gap by estimating the human health effects of urban heat on mortality and morbidity across LA county at the zipcode level. We gather social vulnerability scores using socio-demographic data and incorporate measures of prolonged heat exposure derived from high-resolution, near-surface air temperature data into fixed effects and polynomial regression models. Our findings are generally consistent with past work in the literature and reveal that our measures and models may be applicable for informing mitigation measures at the local level.

## I. Introduction

Since the start of the Industrial Revolution, Earth's global climate has increased by at least 1.1° C, driven largely and unequivocally by anthropogenic activities ranging from the burning of fossil fuels to the clearing of natural habitats (1, 2). The negative consequences of global climate change are wide-ranging: increased occurrences of extreme weather events, greater risk of food insecurity, involuntary migration and displacement, increased mortality and morbidity rates, and more (1). Extreme heat in particular has been an area of interest among researchers and policymakers, due to its well-established effects on public health, including exacerbating pre-existing health conditions such as cardiovascular disease and asthma and increasing morbidity and mortality rates such as those caused by heat exhaustion and stroke (3). Indeed, heat waves have caused more deaths than all other extreme weather events combined in the past decades, both in the United States and across the world, and are expected to become more frequent, intense, and deadly in the future (4, 5, 6). The World Health Organization and the National Institute of Environmental Health Sciences further identified “adaptation opportunities that can reduce the human health costs of climate change ... as a global research priority of the twenty-first century” (7).

In cities and suburbs, extreme heat is amplified due to the urban heat island (UHI) effect. In the US, for example, urban areas experience daytime temperatures 0.5°–4.0°C higher and nighttime

temperatures 1.0°–2.5°C higher than those in nearby non-urban areas. Many features of the built environment contribute to these UHIs, including lower vegetation levels, less reflective surfaces, urban geometries that trap heat, and human activities that release heat, such as cooling buildings and driving cars (8). The elevated temperatures from UHIs additionally increase energy demand, energy consumption, greenhouse gas emissions, and air pollution levels, all of which contribute to climate change. Climate change and UHIs additionally interact such that high urban temperatures are intensified due to warming trends, resulting in greater annual heat wave frequencies and lengths as well as increased health risks (3, 9). As cities become more densely populated, UHIs are expected to intensify, with the World Bank projecting that nearly 70% of the world's population will live in cities by 2050, compared to the current 56% (1, 8, 10, 11).

While the negative health effects of climate change, UHIs, and extreme heat pose a substantial risk to the general public, it is crucial to recognize the disproportionate impacts on historically disadvantaged communities and vulnerable populations. These groups include the elderly, who are more prone to adverse health conditions and more likely to live in isolation; young children, whose bodies are still developing; those who tend to work outdoors, who are more exposed to heat stress and air pollution; and those with pre-existing health conditions, such as diabetes, cardiovascular disease, obesity, and mental health conditions (9, 12). Low-income communities and people of color are also more vulnerable to climate- and heat-related stresses, tending to live in areas that are denser, have poorer air quality, and have less vegetation compared to high-income communities, which can exacerbate health risks including increased heat-related deaths (1, 4, 5, 6). Additional factors affecting vulnerability include lack of access to air conditioning and electricity, low levels of education, poor housing conditions and overcrowding, language barriers, and an overall lack of access to resources to adequately respond to extreme heat (9, 13).

These factors both exacerbate and are influenced by social and racial hardships, a relationship that has been extensively documented by numerous studies (13). One study conducted by Hoffman et al. examined the relationship between historic housing policies and the disproportionate exposure to extreme heat, finding that the impacts of redlining, or the historic practice of denying loans, mortgages, and home ownership based on racist appraisals of financial risk, continue to harm primarily low-income communities and communities of color. In particular, formerly redlined areas showed land surface temperatures 7°C higher than those in non-redlined areas across the United States (6). Another study by Egeded et al. linked historic redlining practices to health and social consequences including increased risk of diseases such as diabetes and hypertension and to limited social advancement in the form of income and education (14). Indeed, these historic and environmental injustices underscore the need for targeted policies and mitigation strategies to address their impacts.

To examine the health effects of extreme temperatures, studies often estimate temperature-mortality relationships, which yield interpretable findings for decisionmakers. In this branch of the literature, studies by Carleton et al., Vicedo-Cabrera et al., and Gasparrini et al. all find similar U-shaped relationships between temperature and mortality rates, where mortality rates are high at very low temperatures, low at moderate temperatures, and high again at extremely high temperatures ([15](#), [16](#), [17](#)). Temperature-morbidity relationships, although less investigated than temperature-mortality relationships, are similarly helpful, with past studies generally finding contrasting behaviors between mortality and morbidity estimates at extreme temperatures. One study by Yuan et al., for example, found increased but differing risk of both mortality and morbidity in response to cold temperatures but found increased risk of morbidity and almost no risk of mortality for hot temperatures across Japan ([18](#), [19](#)). Importantly, these relationships are unique to given locations, affected by local variables including atmospheric humidity and socioeconomic factors ([20](#)). In particular, when observing the temperature-mortality relationship across demographics, Carleton et al. found that the relationship is more pronounced in populations with lower incomes, suggesting that climate change will increase mortality rates most severely in poor countries. These findings support the consensus that the impacts of extreme heat on public health are felt disproportionately by poor regions across the world ([15](#)).

With comparable temperature increases of  $0.5^{\circ}$ – $4.0^{\circ}\text{C}$  and  $1.0^{\circ}$ – $2.5^{\circ}\text{C}$ , respectively, UHIs and climate change both contribute to extreme heat and its associated human health effects ([2](#), [7](#)). Despite this comparability, however, the impacts of urban heat have received relatively less attention from the public and policymakers, when empirical estimates can help decisionmakers evaluate the influence of the phenomena in their location. To address this gap, this study examines the human health effects of urban heat in LA county, the most populated county in the United States, at the zipcode level, using socio-demographic, mortality and morbidity, and high-resolution, near-surface air temperature data. In particular, we regress annual mortality and morbidity rates on measures of prolonged heat exposure derived from the temperature data, estimating models separately across age groups and mortality and morbidity causes. We anticipate that the negative health impacts of prolonged heat exposure will exceed those of isolated heat exposure, particularly in groups that are more sensitive to extreme heat (e.g., the elderly). We ultimately aim to contribute to ongoing research in empirically understanding the impacts of extreme events, while providing resources for local communities and decisionmakers.

## II. Methods

### Data

#### *Temperature data*

Bins for daily average, minimum, maximum, diurnal range, and maximum-diurnal range temperatures, as well as counts for annual heatwave days, were gathered at the zipcode level.

Daily minimum and maximum near-surface air temperatures were gathered from Zhang et al.’s global gridded dataset, offering 1 kilometer spatial resolution from 2003 to 2020 using ground station measurements and remotely-sensed data (21) . Daily minimum temperature is defined as midnight land surface temperature, and daily maximum temperature is defined as daytime land surface temperature. Extracting from LA-specific data, daily one-degree temperature bins for each year from 2003 to 2020 were created for minimum, maximum, average, and diurnal range temperatures, as well as for a maximum-diurnal range temperature interaction. Here we define daily average temperature as the average of the corresponding daily minimum and maximum temperatures and diurnal range temperature as the difference between the corresponding daily maximum and minimum temperatures. The maximum-diurnal range temperature interaction is defined as  $T_{\max} / \text{DiurnalRange}$ , where  $T_{\max}$  is the daily maximum temperature, to quantify the number of days that have both a high maximum temperature and a low diurnal range temperature, which may result in greater risk of mortality or morbidity.

The number of heatwave days for each year was recorded using the EPA’s definition of heatwaves as “a period of two or more consecutive days where the daily minimum apparent temperature ... is higher than the 85th percentile of historical July and August temperatures for that city” (22). Here we use a single threshold for LA county aggregated from pixel-level thresholds, derived by Druckenmiller et al. from 1981 to 2010 PRISM data. We use a single threshold rather than city-specific thresholds because we are not conducting large-scale impact comparisons.

To aggregate the above measures from the pixel level to the zipcode level, we implemented a weighting by area approach, in which the proportion of each pixel cell that overlapped with a zipcode’s area was used as the weight to compute a weighted sum for each zipcode. This approach helps increase the accuracy of the aggregated measures given that the gridded dataset’s spatial resolution of 1 kilometer is coarse relative to the size of the average LA zipcode.

#### *Socio-demographic data*

We curated a dataset of zipcode-level socio-demographic variables using the American Community Survey’s (ACS) 2022 five-year estimates to compute social vulnerability scores. These variables were selected after an extensive literature review conducted by Shreevastava et al., and includes counts encompassing living conditions, social isolation, age, race, health, education, and transportation barriers, all of which have been found to influence responses to extreme temperatures. The 18 variables collected so far, out of the 26 used by Shreevastava et al., are shown in Table 1 (27).

Table ID	Indicators	Description
B25040	Solar	Population using solar energy for house heating fuel.

DP02	ForeignBorn	Foreign born population
DP03	Unemployment, WorkOutdoors	Unemployed population and population of outdoor workers (workers in natural resource, construction, maintenance, production, transportation, and material moving occupations)
DP05	TotalPop, WhitePop, BlackPop, AsianPop, NativePop, HispanicLatino, Children, Elderly	Total zipcode, race (white, Black, Asian, Native American, and Hispanic or Latino), elderly (those aged 65 and older), and children (those under 18) populations
S1101	Renting, LiveAlone, LiveAloneElderly	Renting, live alone, and both live alone and elderly (those aged 65 and older) populations
S1501	LessThanHS, MaxHS	Less than high school education and maximum high school education populations
S1701	ExtremePoverty	Population living in extreme poverty, or those whose income is below 50% of their poverty level ( <a href="#">23</a> )
S2501	ManyOccupants, Overcrowded	Population living with many occupants and population living in overcrowded conditions, defined as more than 1.01 people per room ( <a href="#">24</a> )

**Table 1** ACS data used to curate our socio-demographic dataset. The table ID indicates the ACS table used, and the indicator column indicates the variables extracted from that table. These same indicators are used in Figure 5. The description column defines the indicators.

#### Health data

We additionally curated a health dataset of hospital emergency department (ED) visits (morbidity) and death profiles (mortality) at the zipcode level, obtaining data for both variables from the California Department of Public Health (CDPH) ([25](#), [26](#)).

The annual morbidity records consisted of hospital information, patient information, age groups, number of visits, principal diagnosis groups, and principal external cause of injury groups at facilities across California from 2005 to 2022. Only hospital zipcodes, age groups, number of visits, and principal diagnosis groups from 2005 to 2020 were pulled for the final dataset. Age groups were further aggregated into the following groups: 0-9, 10-59, 60-79, and 80 and over. Since they varied slightly from year to year, principal diagnosis groups were adjusted into the

following 18 groups: Perinatal Disorders; Pregnancy, Birth, and Puerperium; Congenital Anomalies; Blood and Bloodforming Organs; Circulatory; Digestive; Endocrine; Respiratory; Nervous and Sensory; Musculoskeletal; Neoplasms; Genitourinary; Infections; Injuries and Poisoning; Mental Illness; Skin; Symptoms; and Other. These groups were chosen such that their corresponding International Classification of Diseases (ICD) diagnosis and procedure codes were consistent across all years, where the codes used for each principal diagnosis group were provided by the CDPH. All counts were standardized per 100,000 population, using zipcode population data from the (ACS). Notably, some zipcodes yielded rates larger than 100,000 due to discrepancies between reported ED visits and zipcode populations.

However, because morbidity counts were recorded at the hospital level, many LA zipcodes were not represented. To preserve the quality of the data, missing zipcode rates were imputed using a catchment grouping approach, with each catchment group consisting of a represented zipcode and a set of non-represented zipcodes, determined by the shortest distance between their centroids. Each zipcode in that group was then assigned a new rate determined by the represented zipcode's morbidity counts divided by the sum of populations of all zipcodes in the catchment group. This approach mitigates error from the initial overestimation of ED visit counts that stemmed from our assumption that hospital visit counts were representative of the hospital's zipcode visit counts. In reality, it is highly likely that hospitals in a given zipcode are visited by nonresidents of that zipcode, and we therefore use the population of the entire catchment group rather than that of a single zipcode to calculate morbidity rates. Imputed all-age all-cause morbidity rates are shown in Figure 1.

The mortality records consisted of annual all-age all-cause counts, age-specific all-cause counts, all-age cause-specific counts, and all-age, all-cause, gender-specific counts from 1989 to 2022. Only the all-age all-cause, age-specific all-cause, and all-age cause-specific counts from 2005 to 2020 were pulled for the final dataset. Age groups were further aggregated into the following groups: 0-4, 5-14, 15-64, 65-84, and 85 and over. The 14 cause of death categories, determined by the CDPH using ICD codings, were kept the same, labeled as the following: Accidents, Alzheimers, Homicide, Cerebrova, Cirrhosis, Respiratory, Diabetes, Heart, Hypertension, Influenza and Pneumonia, Suicide, Neoplasms, Nephrosis, and Parkinsons. All counts were standardized per 100,000 population using ACS zipcode population data to yield mortality rates.

Although data was present for each zipcode in LA County, many zipcodes were missing data for certain categories and groups. To impute the obtained data, a catchment grouping approach was implemented on each category, in the same way as for the morbidity data. Imputed all-age all-cause mortality rates are shown in Figure 2.

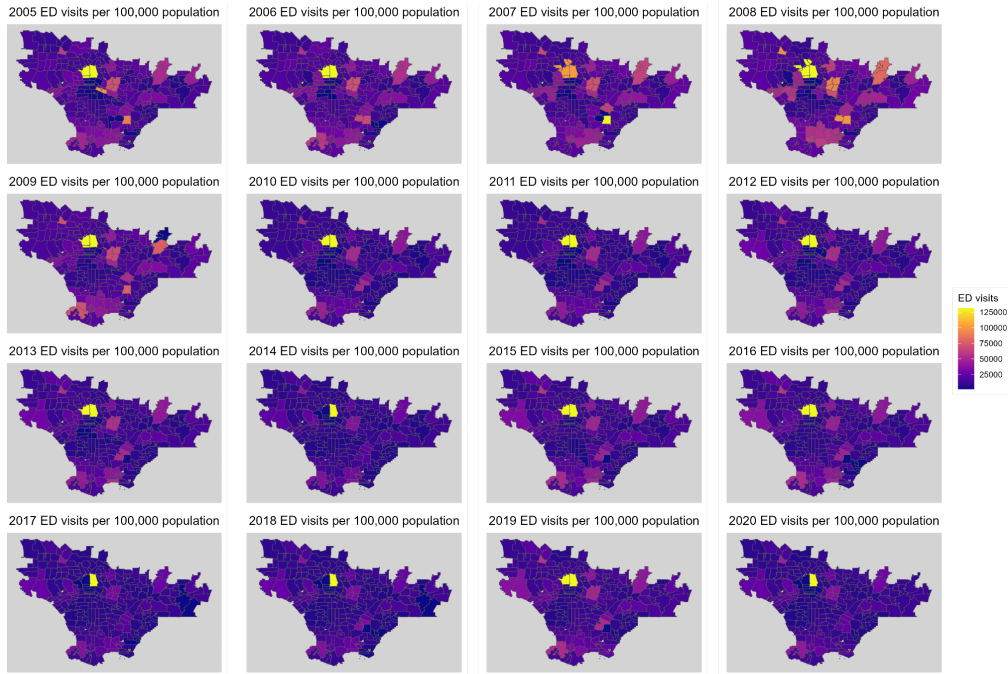


**Figure 1** Total annual ED visit rates per zipcode from 2005 to 2020. The trend in ED visit rates, or morbidity rates, is relatively constant.

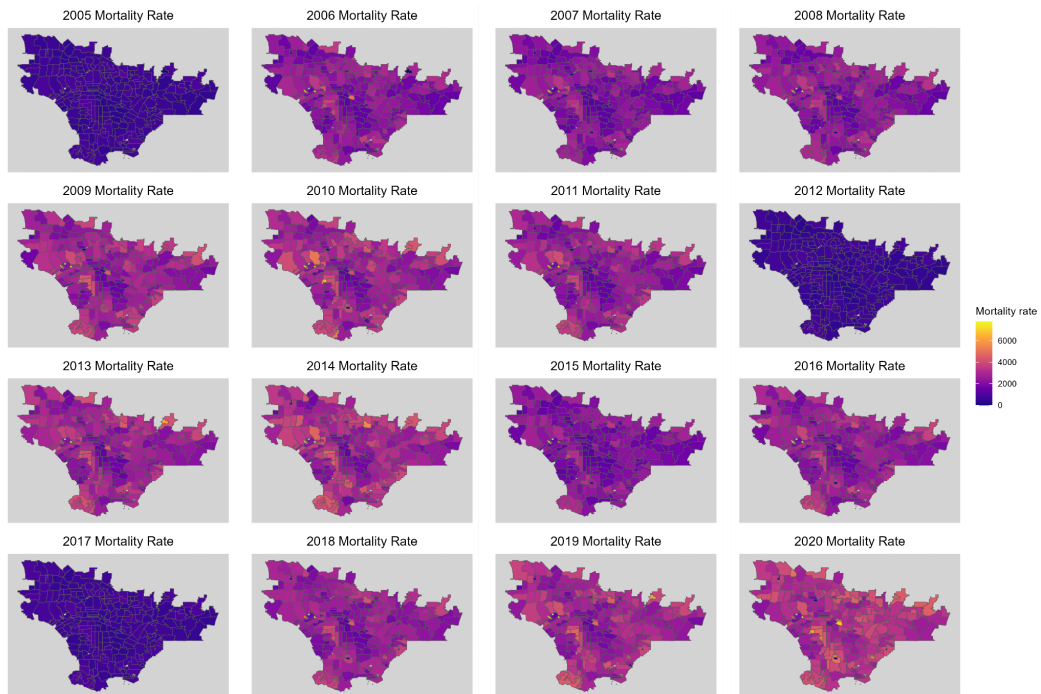


**Figure 2** Total annual mortality rates per zipcode from 2005 to 2020. A general upward trend in mortality rates can be observed.

## Empirical approach

### *Principal components analysis*

Following the methodology developed by Shreevastava et al., principal components analysis (PCA) was performed using scikit-learn's PCA package, applying singular value decomposition (3, 4, 5, 27). Based on their explained variances, the first four principal components (PCs) were selected to obtain a single social vulnerability score, computed by weighting each of the standardized PCA scores  $PC_i$  with its variance  $var_i$ , as shown in Equation 1.

$$(1) \text{ Vulnerability} = \frac{PC_1 * var_1 + PC_2 * var_2 + PC_3 * var_3 + PC_4 * var_4}{var_1 + var_2 + var_3 + var_4}$$

After removing outliers, we interpreted each principal component in terms of the selected socio-demographic variables to validate the interpretability of the vulnerability score. We obtained loadings using scikit-learn, which returns the coefficients of the linear combination of variables that define each principal component (8).

### *Regression analysis*

After aggregating one-degree bins into five-degree bins for daily average, minimum, maximum, diurnal range, and maximum-diurnal range temperatures, we implemented a linear two-way fixed effects model on each of the binned data, controlling for year and zipcode. Annual mortality and morbidity rates were regressed separately across age groups and mortality and morbidity causes. To avoid collinearity, the 10-15 °C bin was omitted from the model and used as the reference bin, allowing changes in annual mortality or morbidity rates per additional day in a given bin to be interpreted relative to the 10-15 °C bin. For maximum-diurnal range bins, which ranged from 0-5 in one-value intervals, the 2-3 value bin was used as the reference. A cubic polynomial model was also implemented on the heatwave count data, allowing for non-linear estimates. Finally, the two above models were combined to regress rates on both the heatwave counts and the individual binned data.

## **III. Results**

### Principal components analysis

The social vulnerability scores, as depicted in Figure 4, showed spatial patterns consistent with previous findings, with several zipcodes in central LA emerging as the most vulnerable (27). Indeed, the loadings used to derive these scores suggest that the scores can be interpreted as indicators of heat sensitivity, with the most significant contributors being variables encompassing living conditions, occupation, poverty, employment, nationality, age, and race. As illustrated in Figure 5, the first PC (PC1) is positively correlated with variables related to living conditions, occupation, education, and race but negatively correlated with those related to age, and nationality, while the second PC (PC2) is positively correlated with living conditions, poverty, nationality, and race but negatively correlated with age. The third PC (PC3) is positively correlated with unemployment but negatively correlated with education and occupation, and

lastly the fourth PC (PC4) is positively correlated with age but negatively correlated with certain living conditions.

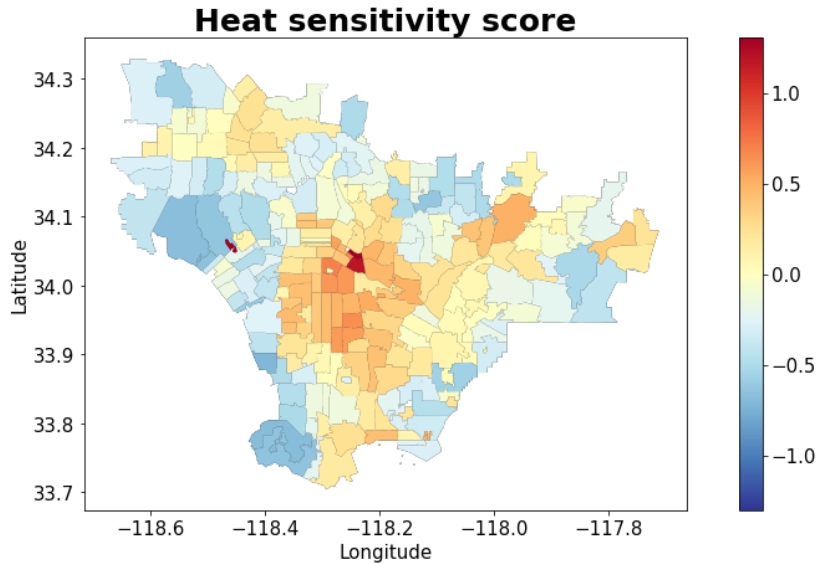


**Figure 4** Vulnerability scores for each zipcode using 2022 socio-demographic data. A high score indicates high vulnerability to heat as a function of socio-demographic variables including living conditions, education levels, occupation, employment, nationality, age, and race.

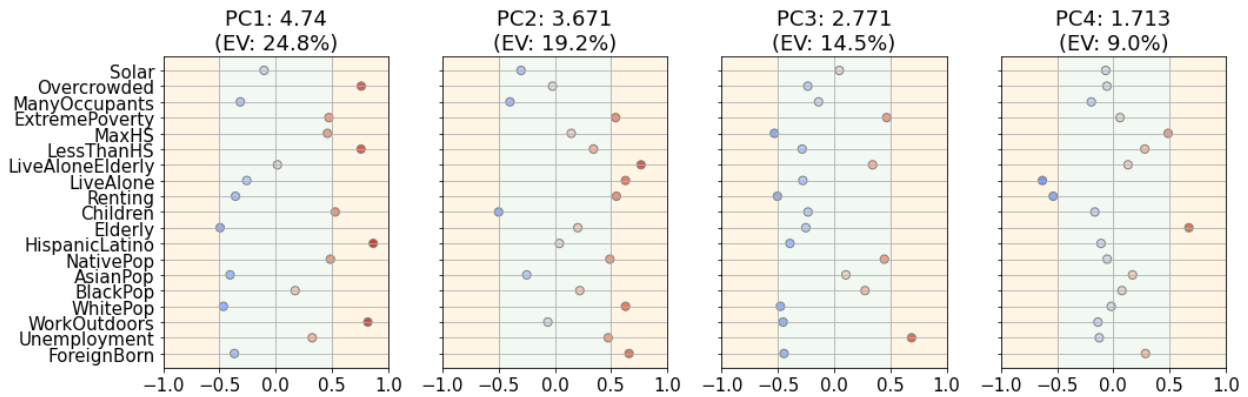


**Figure 5** Loadings for each principal component. A high loading for a particular variable indicates a high contribution to the principal component. Variances and variance ratios for each principal component are included in the graph titles.

### Regression analysis

#### *All-cause*

We found clear distinctions between all-cause mortality and all-cause morbidity estimates after regressing the health data separately across our five measures: average, minimum, maximum,

diurnal range, and maximum-diurnal range temperature bins. Although the typical U-shaped relationship was not recovered, annual all-cause mortality rates increased in response to an additional day with high average and minimum temperatures (temperatures greater than 35 °C and 30 °C, respectively), relative to our selected reference bin of 10-15 °C. In contrast, annual mortality rates decreased in response to an additional day with low maximum and maximum-diurnal range values (temperatures less than 5 °C and values less than 0, respectively), with almost no change in response to extreme hot temperatures or values. Maximum-diurnal range temperature bins yielded an increase in mortality rates at least 12 times greater than that yielded by just the maximum temperature bins. For just the diurnal range temperature bins, annual mortality rates decreased at moderate to high temperatures (temperatures greater than 25 °C) and changed minimally at other temperature ranges (Figure 6).

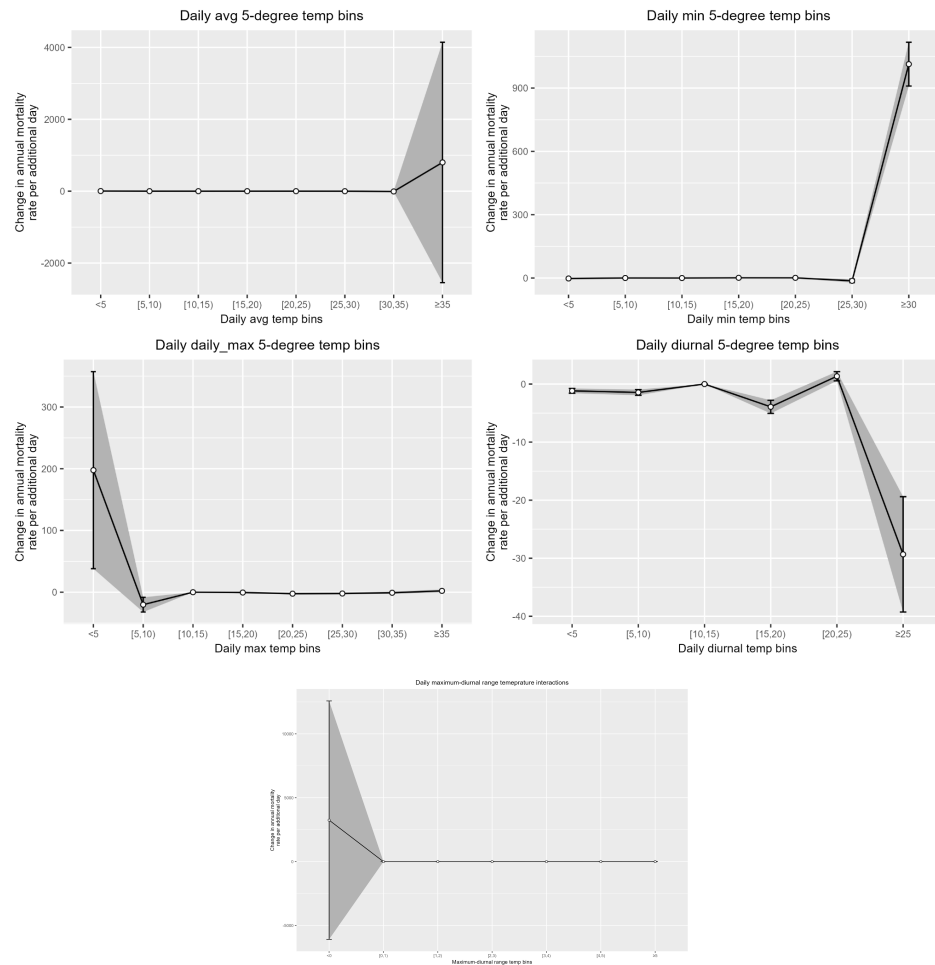


**Figure 6** All-age all-cause mortality estimates for average, minimum, maximum, diurnal range, and maximum-diurnal range temperature bins. The coefficients of each bin yielded from the fixed effects regression, interpreted as the change in annual mortality rate per additional day in the bin relative to the 10-15 °C bin, are plotted against the binned data. The gray shaded regions indicate the standard error associated with each coefficient.

Annual all-cause morbidity estimates generally varied from all-cause mortality estimates. Similar to mortality, morbidity rates increased in response to high average temperatures but, in contrast, decreased in response to high minimum temperatures, with no significant changes at other temperature ranges for both measures. Morbidity rates also increased only at low ranges for maximum temperature bins and maximum-diurnal range temperature bins, which yielded an increase in rates at least 8 times higher than that yielded by just the maximum temperature bins. For just the diurnal range temperature bins, morbidity estimates followed trends similar to those yielded by average temperature bins, with slight increases and decreases at moderate temperatures; only average, maximum, and maximum-diurnal range measures yielded trends consistent between both mortality and morbidity estimates (Figure 7).

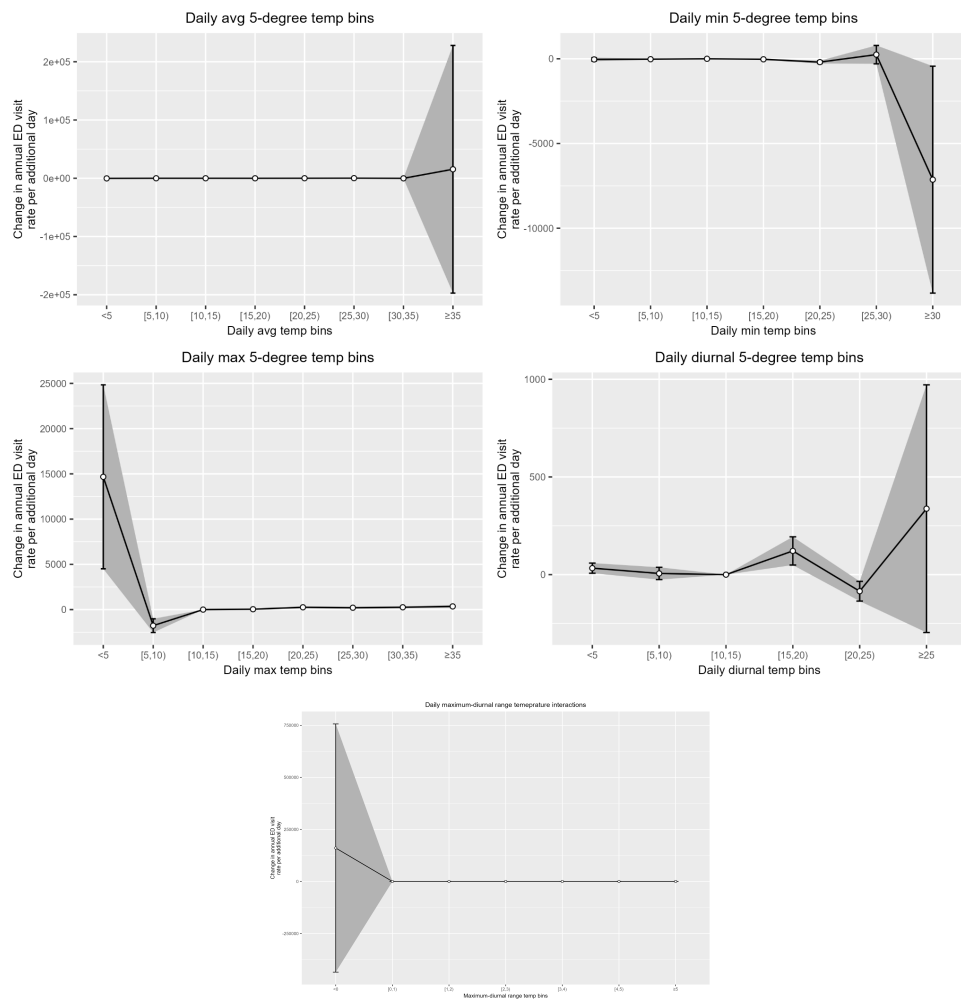


**Figure 7** All-cause morbidity estimates for average, minimum, maximum, diurnal range, and maximum-diurnal range temperatures. The coefficients of each bin yielded from the regression are plotted against the binned data, where the gray shaded regions indicate the standard error associated with each coefficient.

To assess the robustness of these models, we experimented with bins of varying widths for average, minimum, maximum, and diurnal range temperature measures, comparing four-degree and six-degree bins against our initial five-degree bins. All-cause mortality and morbidity estimates for the two additional bin widths are shown in Figures 8 and 9, which illustrate trends that vary significantly from those estimated using five-degree temperature bins. For instance, in response to average temperatures with four degree bins, mortality rates increase at low temperatures and decrease at high temperatures, while morbidity rates decrease at both low and high temperatures. Estimates vary similarly for a majority of the measures.

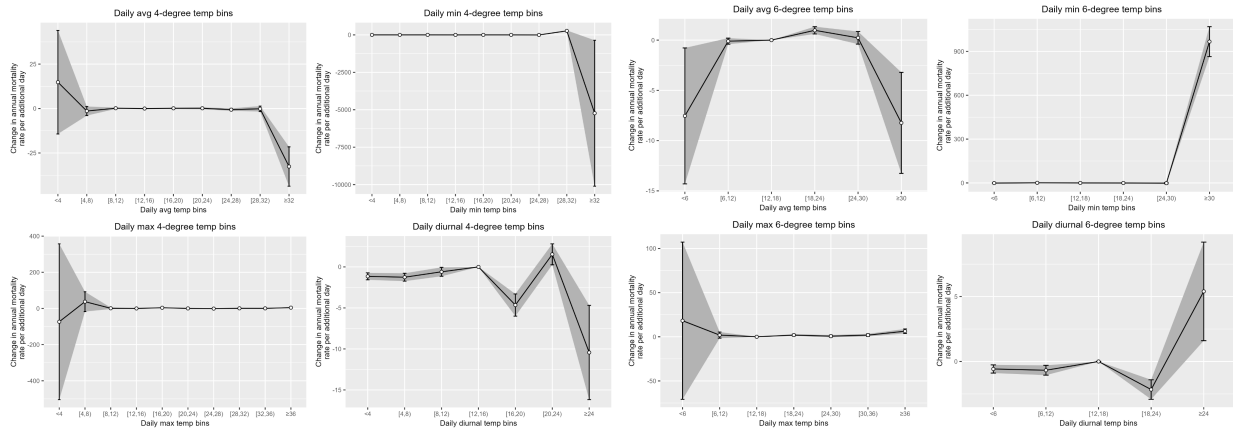


**Figure 8** All-cause mortality estimates as a function of four-degree and six-degree temperature bins. Trends vary across all four measures.

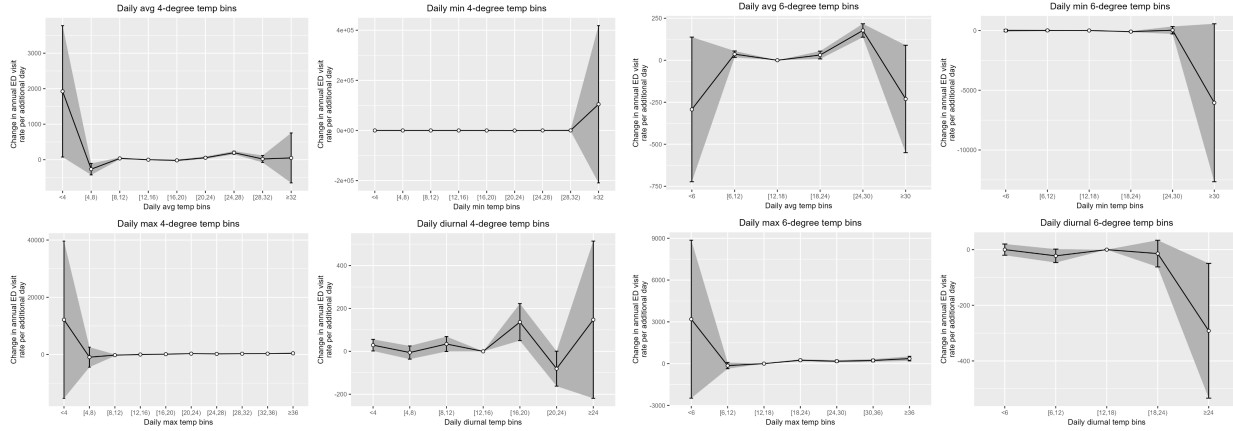


**Figure 9** All-cause morbidity estimates as a function of four-degree and six-degree temperature bins. Trends vary across average, minimum, and diurnal range temperature measures.

*Age-specific*

Before running the model on age-specific mortality and morbidity rates, certain age groups were merged to avoid data containing zero variance, preventing the regression model from yielding invalid coefficients. In particular, the 0-4 and 5-14 mortality age groups were aggregated into a 0-14 age group for average, minimum, maximum, and diurnal range temperatures. The resulting age groups exhibited trends that varied most significantly for mortality rates. As illustrated in Figure 10, mortality rates increased the most at cold temperatures and low values for those 85 and older in response to maximum and maximum-diurnal range temperature bins, following trends similar to all-cause, all-age mortality.

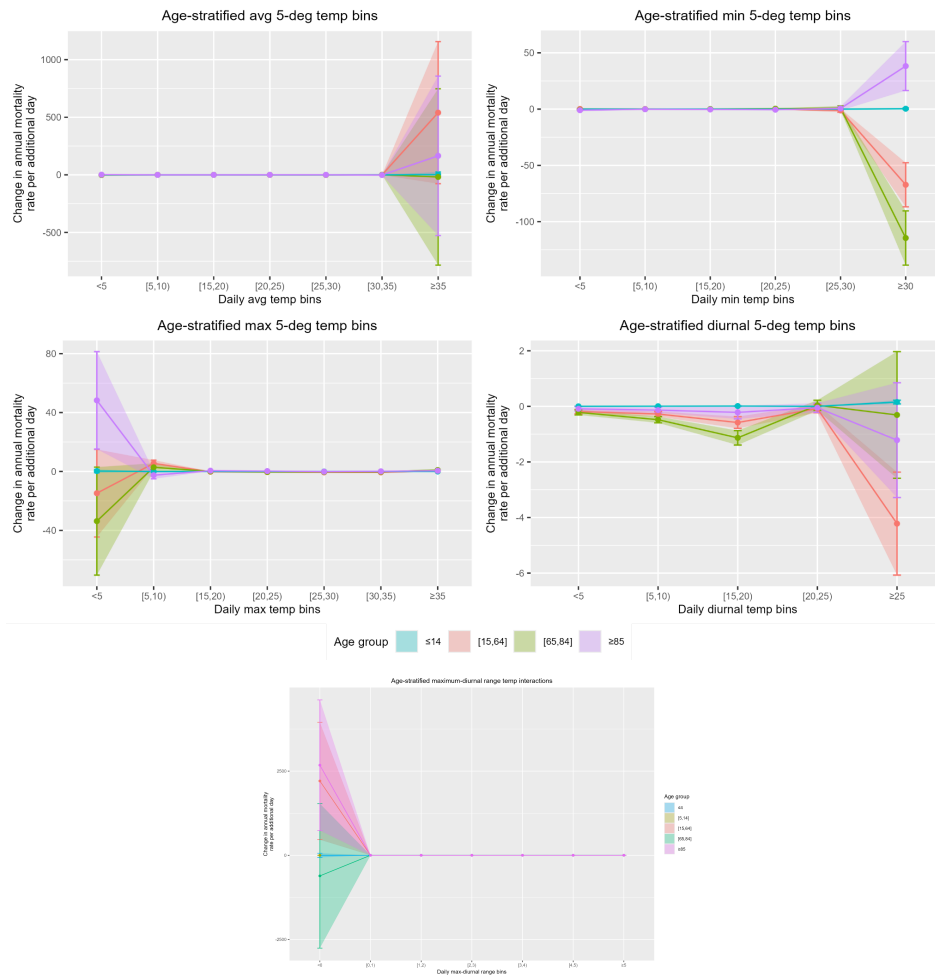


**Figure 10** *Age-stratified mortality estimates.* Age groups for certain measures were further aggregated to avoid data with non-zero variance and yield more accurate results from the regression analysis. Trends across groups varied, with the older age groups generally experiencing greater impacts and the youngest age groups experiencing almost no impacts.

However, while trends across age groups were generally consistent for maximum-diurnal range temperature bins, the remaining age groups for just maximum temperatures experienced either a

decrease in rates or almost no change, diverging from all-cause, all-age trends. Those 85 and older were also impacted the most severely in response to high minimum temperatures, with mortality rates increasing for this age group only and diverging from all-cause, all-age trends. In contrast, for average and diurnal range temperatures, the 15 - 64 age group was impacted the most severely, with mortality increasing and decreasing, respectively, in line with all-cause, all-age trends. In each of the measures, the young age groups experienced almost no change in mortality rates.

Compared to mortality estimates, morbidity estimates across age groups were much more consistent with each other and with all-cause, all-age morbidity trends. For all measures, the 10-59 age group was impacted most severely, with those 80 and older experiencing the least amount of change in morbidity rates. For instance, when regressed on average temperatures, only the 10-59 group experienced an increase in morbidity rates, while the remaining age groups experienced a slight decrease. The youngest age group, those 9 and below, experienced the second most severe impacts, followed by the 60-79 age group as illustrated by the minimum and maximum temperature bins (Figure 11).

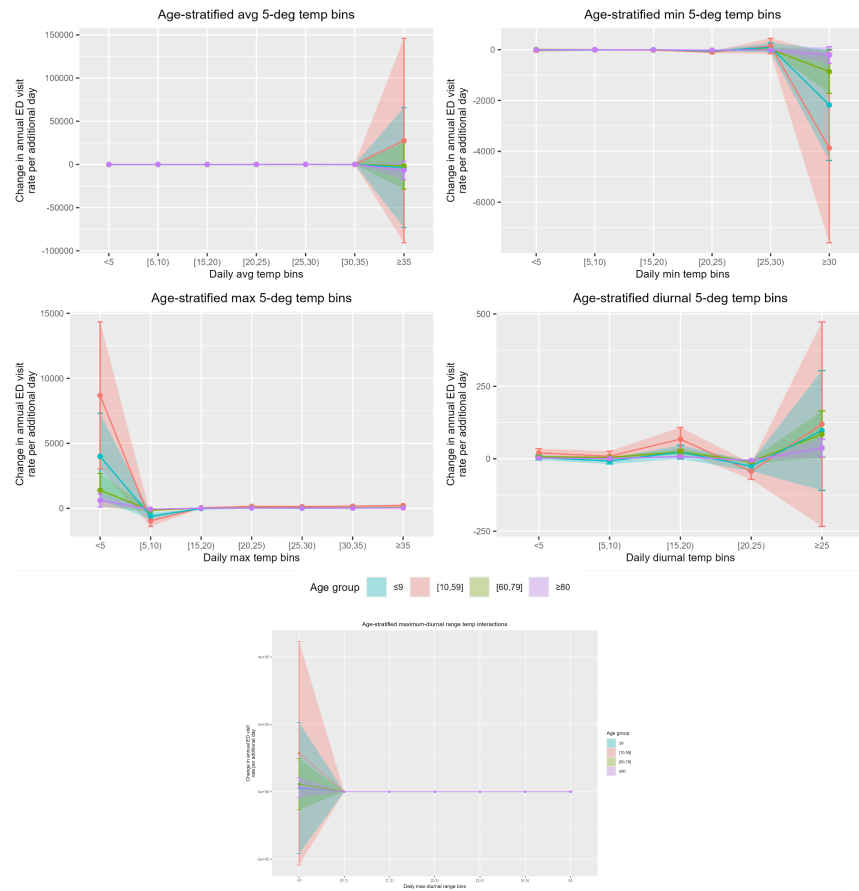


**Figure 11** *Age-stratified morbidity estimates.* Trends across groups are generally consistent, with the two youngest age groups experiencing the greatest impacts and the oldest age group experiencing the least impacts.

### Cause-specific

Five causes were selected from the 14 total causes of mortality and the 18 total causes of morbidity, encompassing illnesses with rates that have been found to increase at extreme temperatures as well as illnesses with rates that we expect to change minimally at extreme temperatures. For mortality estimates, these five causes include accidents, heart, hypertension, Parkinsons, and respiratory diseases; as illustrated in Figure 12, all-age cause-specific mortality estimates generally varied from all-age all-cause estimates, with hypertension and respiratory-related mortality rates decreasing at high temperatures for average temperature bins, though heart-related mortality rates did increase. In response to minimum temperature bins, mortality decreased at high temperatures for heart, hypertension, and respiratory-related death, though only slightly at rates ranging from 2 to 20 counts per 100,000 population. In response to maximum temperature bins, mortality increased at low temperatures for heart and hypertension-related death but decreased for respiratory-related death, at rates ranging from 0 to 30 counts per 100,000 population. Accidents-related and, in particular, Parkinsons-related mortality changed only slightly across average, minimum, and maximum temperatures, at rates ranging from 20 to 50 and 0 to 5 counts per 100,000 population. Cause-specific estimates for the remaining measures and for additional causes are included in the appendix.

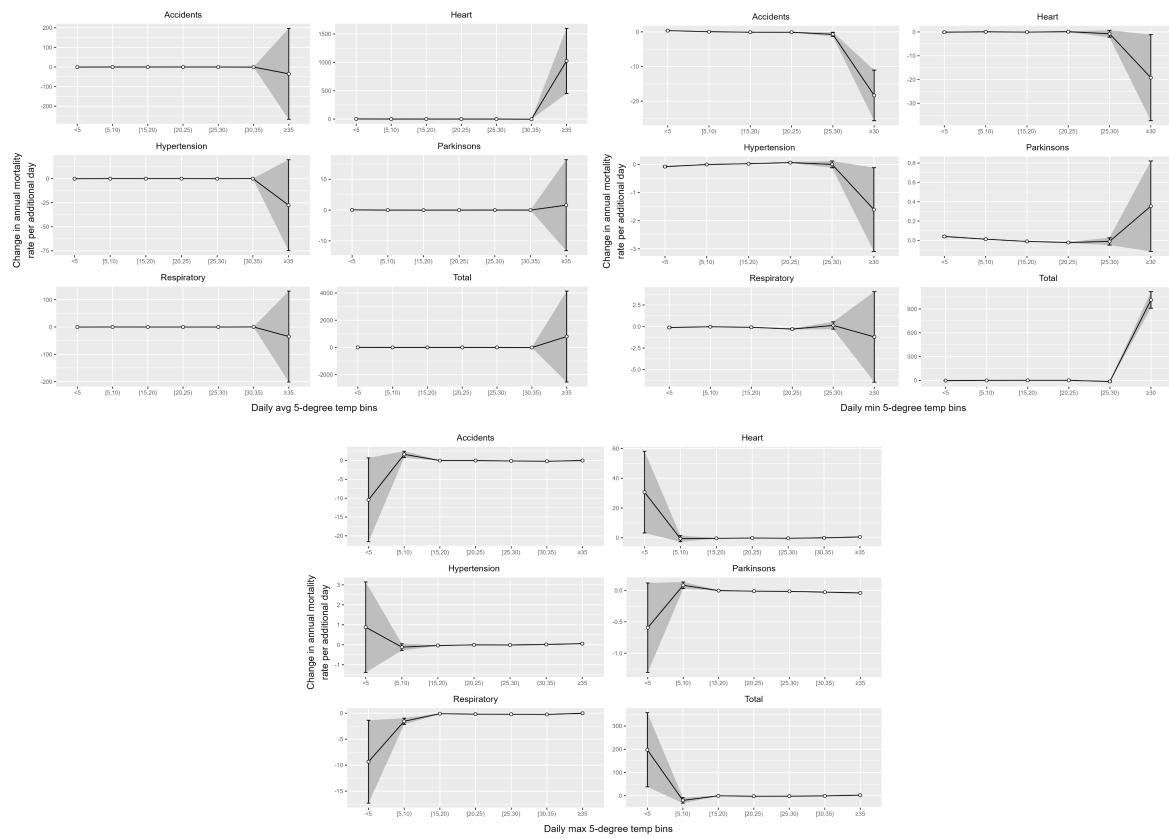


**Figure 12** Selected cause-specific mortality estimates for average, maximum, and minimum temperatures. Changes in mortality rates for accidents and Parkinsons-related mortality are small, while changes in the remaining selected

causes vary. The “total” title indicates all-age, all-cause estimates. Estimates for the remaining measures and causes are included in the appendix.

Compared to mortality, all-age cause-specific morbidity estimates were less varied and more closely followed all-age all-cause trends. Circulatory, injuries and poisoning, respiratory, symptoms, and illnesses classified as “other” were selected as our five causes. For average temperature bins, which showed an increase in all-age all-cause morbidity at high temperatures, ED visits as a result of circulatory illnesses decreased at the same high temperatures, but indeed increased for ED visits caused by respiratory illnesses, injuries and poisoning, symptoms, and illnesses categorized as “other.” Morbidity rates similarly followed all-age all-cause trends for both minimum and maximum temperature bins, with rates decreasing at high temperatures and increasing at low temperatures, respectively, except for circulatory-related ED visits when regressed on maximum temperatures, which showed a slight decrease in rates at low temperatures. Morbidity estimates were generally much larger than mortality estimates (Figure 13). Cause-specific estimates for the remaining measures and for additional causes are included in the appendix.

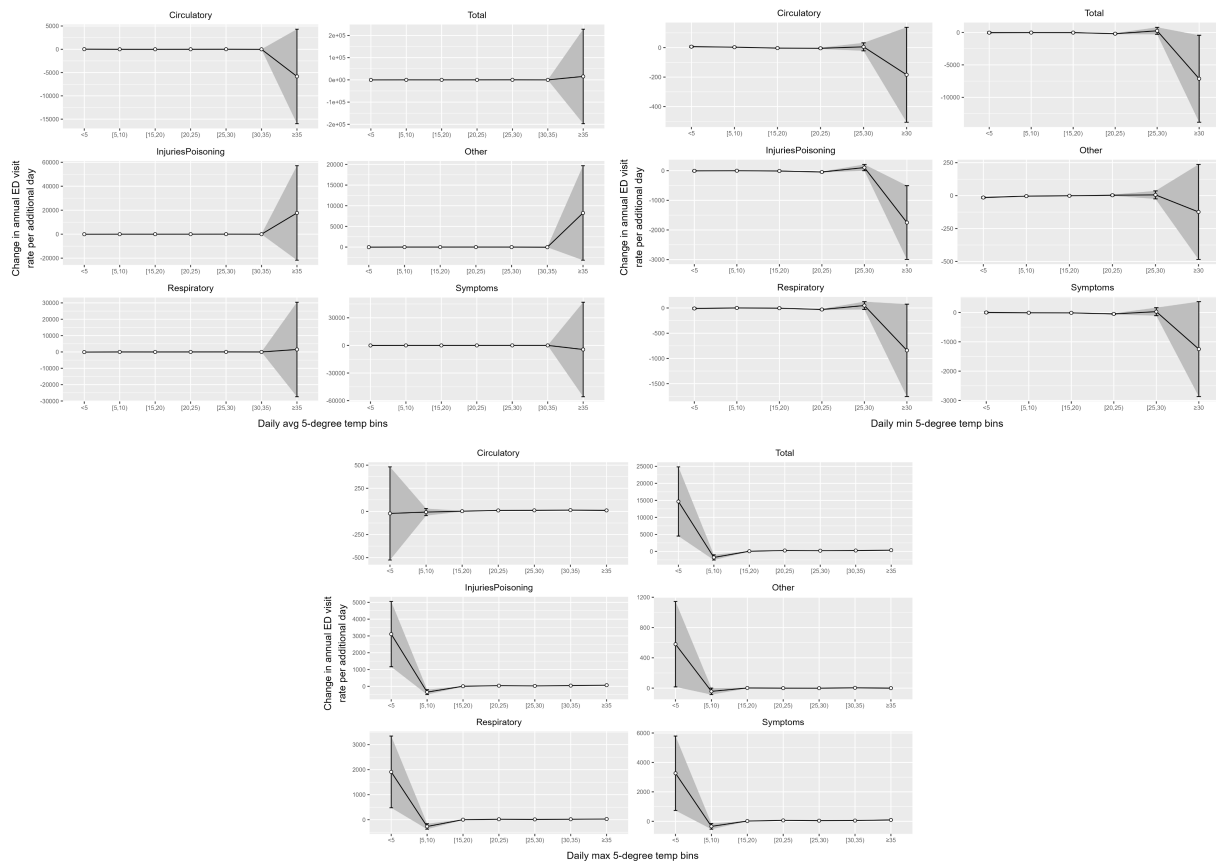


**Figure 13** Selected cause-specific morbidity estimates for average, maximum, and minimum temperatures. Changes in morbidity rates for all selected causes generally follow all-age all-cause estimates, as indicated by the “total” graph. Estimates for the remaining measures and causes are included in the appendix.

## Heatwaves

The polynomial model regressed on heatwave counts yielded varying results for mortality and morbidity. The mortality-heatwave relationship yielded a negative cubic trend, while the morbidity-heatwave relationship yielded a positive cubic trend, as shown in Tables 2 and 3, respectively. To assess the robustness of the model, we regressed the health data on heatwave counts alongside each of the binned data. The resulting coefficients showed relationships consistent with those yielded from regressing mortality and morbidity on just heatwaves. Results for these additional models are included in the appendix.

Variable	Coefficient	Standard error	P-value
Heatwave	-83.3804	18.3167	5.48e-06
Heatwave <sup>2</sup>	14.9883	3.0753	1.14e-06
Heatwave <sup>3</sup>	-0.7995	0.1578	4.23e-07

**Table 2** Resulting coefficients for mortality rates regressed on heatwave counts. The coefficients indicate a negative cubic relationship.

Variable	Coefficient	Standard error	P-value
Heatwave	2322.31	1170.75	0.0474
Heatwave <sup>2</sup>	-385.50	196.57	0.0499
Heatwave <sup>3</sup>	16.47	10.08	0.1024

**Table 3** Resulting coefficients for morbidity rates regressed on heatwave counts. The coefficients indicate a positive cubic relationship.

## **IV. Discussion**

The principal components analysis framework can be utilized by future work to curate datasets and generate scores with greater temporal coverage, such as from 2005 to 2020 to align with the health data, to enable these scores to be more readily applied, such as by incorporating them into regression analyses. These scores, especially in a time series, can be helpful in identifying zipcodes that are most at risk to implement targeted extreme heat mitigation strategies.

With the regression analysis, we find varying outcomes for morbidity and mortality estimates regressed on multiple measures of heat exposure. As shown in Figure 6, although the typical U-shaped mortality-temperature relationship was not fully recovered, the average and minimum bins as well as the maximum and maximum-diurnal range bins generally each yielded one tail of

the U-shaped relationship across all-age all-cause, age-specific all-cause, and all-age cause-specific rates for both mortality and morbidity, indicating that certain bins may uncover insights that are obscured by others. The diurnal range bins in particular produced unexpected results, with mortality rates decreasing at high temperatures and morbidity rates increasing under the same conditions. These findings may indicate that large diurnal range temperatures are generally not life-threatening but still detrimental to health, increasing ED visits. Mortality rates might decrease as a result of people seeking treatment and managing their symptoms effectively, but future work should examine the relationship between diurnal range temperatures and extreme heat more closely, especially due to limited related work in the literature. The results further indicate that it may be helpful to examine multiple different measures to comprehensively assess health effects, and since mortality estimates and morbidity estimates varied significantly, it may be important to assess both health indicators separately.

Age-specific estimates for mortality and morbidity showed that the elderly were indeed most heavily impacted for some measures, consistent with findings in the literature. However, young age groups experienced almost no change in rates across all measures for mortality, and middle-aged groups for both mortality and morbidity (those aged 15-64 and 10-59, respectively) were impacted most severely for certain measures, indicating that there may be underlying issues with our models (Figures 10 and 11). Cause-specific estimates indicate similar concerns, with respiratory and cardiovascular-related mortality and morbidity estimates experiencing inconsistent changes at high temperatures (Figures 12 and 13).

Indeed, when we varied the width of the bins used in our measures, the model showed trends that differed significantly, underscoring the lack of robustness in our models (Figures 8 and 9). Such inconsistencies are likely explained by the quality of our health data, which underwent large amounts of imputation using the catchment grouping approach. Even after imputing, certain data such as age-specific mortality rates were further aggregated to avoid non-zero variance, and the morbidity data itself was not fully accurate for our purposes; future studies should focus on gathering mortality data with fewer gaps and collecting morbidity data that reflects the number of ED visits within a specific zipcode population, rather than per hospital. This approach may reduce the need for imputation and enhance the overall quality of the data. Improving our datasets may also reduce standard errors for the resulting coefficients and lead to trends that are more consistent with the literature. With the quality of our current data, it is also important to not overinterpret results.

In contrast, the polynomial heatwave model showed results consistent across models where mortality and morbidity were regressed on heatwave counts as well as both heatwave counts and individual temperature bins (Tables 2-13). However, the observed negative cubic mortality relationship was unexpected, and although the positive cubic morbidity relationship was more consistent with work in the literature, we did not anticipate a low to moderate number of

heatwave days to correspond with an increase in rates alongside a high number of heatwave days. Since this behavior was nonetheless consistent across models, it may be possible that there are confounding variables that we did not control for in the models. For example, it may be possible that a greater number of heatwave days correlates with a greater number of people staying indoors, decreasing the risk of heat-related death. Such confounding variables also underscore the importance and potential of incorporating social vulnerability scores into our models, allowing us to control for variables such as living conditions and occupation that influence responses to extreme temperatures.

Future studies examining the health effects of extreme temperatures can benefit from jointly analyzing morbidity and mortality using multiple measures of heat exposure, providing a more comprehensive understanding of the potential consequences of extreme heat. Incorporating measures of prolonged heat exposure, such as heatwaves, can also make estimates more closely aligned with health outcomes and thereby improve their accuracy. Although there are important limitations, our results suggest that extreme temperatures will likely increase both mortality and morbidity rates, with varying impacts on different age groups and those with different health conditions. Additional work on improving our datasets and incorporating social vulnerability scores into our models can help reveal further insights. As climate change progresses, it may also be beneficial to estimate the health effects of extreme temperatures under end-of-century climate change scenarios, allowing for comparisons between present-day impacts of extreme heat and projected impacts of climate change. This approach will ultimately equip decisionmakers with the necessary resources to implement targeted mitigation strategies, enabling communities to better adapt to extreme temperatures.

## V. References

1. Arias, P.A., N. Bellouin, E. Coppola, R.G. Jones, G. Krinner, J. Marotzke, V. Naik, M.D. Palmer, G.-K. Plattner, J. Rogelj, M. Rojas, J. Sillmann, T. Storelvmo, P.W. Thorne, B. Trewin, K. Achuta Rao, B. Adhikary, R.P. Allan, K. Armour, G. Bala, R. Barimalala, S. Berger, J.G. Canadell, C. Cassou, A. Cherchi, W. Collins, W.D. Collins, S.L. Connors, S. Corti, F. Cruz, F.J. Dentener, C. Dereczynski, A. Di Luca, A. Diongue Niang, F.J. Doblas-Reyes, A. Dosio, H. Douville, F. Engelbrecht, V. Eyring, E. Fischer, P. Forster, B. Fox-Kemper, J.S. Fuglestvedt, J.C. Fyfe, N.P. Gillett, L. Goldfarb, I. Gorodetskaya, J.M. Gutierrez, R. Hamdi, E. Hawkins, H.T. Hewitt, P. Hope, A.S. Islam, C. Jones, D.S. Kaufman, R.E. Kopp, Y. Kosaka, J. Kossin, S. Krakovska, J.-Y. Lee, J. Li, T. Mauritsen, T.K. Maycock, M. Meinshausen, S.-K. Min, P.M.S. Monteiro, T. Ngo-Duc, F. Otto, I. Pinto, A. Pirani, K. Raghavan, R. Ranasinghe, A.C. Ruane, L. Ruiz, J.-B. Sallée, B.H. Samset, S. Sathyendranath, S.I. Seneviratne, A.A. Sörensson, S. Szopa, I. Takayabu, A.-M. Tréguier, B. van den Hurk, R. Vautard, K. von Schuckmann, S. Zaehle, X. Zhang, and K. Zickfeld, 2021: Technical Summary. In Climate Change 2021: The Physical Science Basis. Contribution of Working Group I to the Sixth Assessment Report of the Intergovernmental Panel on Climate Change [Masson-Delmotte, V., P. Zhai, A. Pirani, S.L. Connors, C. Péan, S. Berger, N. Caud, Y. Chen, L. Goldfarb, M.I. Gomis, M. Huang, K. Leitzell, E. Lonnoy, J.B.R. Matthews, T.K. Maycock, T. Waterfield, O. Yelekçi, R. Yu, and B. Zhou (eds.)]. Cambridge University Press, Cambridge, United Kingdom and New York, NY, USA, pp. 33–144. doi:10.1017/9781009157896.002.

2. NASA. (n.d.). *World of change: Global temperatures*. NASA. <https://earthobservatory.nasa.gov/world-of-change/global-temperatures>
3. Environmental Protection Agency. (2024, June 3). *Climate Change and Heat Islands*. EPA. <https://www.epa.gov/heatislands/climate-change-and-heat-islands>
4. Berko, J., Ingram, D. D., Saha, S., & Parker, J. D. (2014). Deaths attributed to heat, cold, and other weather events in the United States, 2006-2010. *National health statistics reports*, (76), 1–15.
5. Harlan, S.L., Brazel, A.J., Darrel Jenerette, G., Jones, N.S., Larsen, L., Prashad, L. and Stefanov, W.L. (2007), "In the shade of affluence: the inequitable distribution of the urban heat island", Wilkinson, R.C. and Freudenburg, W.R. (Ed.) *Equity and the Environment (Research in Social Problems and Public Policy, Vol. 15)*, Emerald Group Publishing Limited, Leeds, pp. 173-202. [https://doi.org/10.1016/S0196-1152\(07\)15005-5](https://doi.org/10.1016/S0196-1152(07)15005-5)
6. Hoffman JS, Shandas V, Pendleton N. The Effects of Historical Housing Policies on Resident Exposure to Intra-Urban Heat: A Study of 108 US Urban Areas. *Climate*. 2020; 8(1):12. <https://doi.org/10.3390/cli8010012>
7. Barreca, A., Clay, K., Deschenes, O., Greenstone, M., & Shapiro, J. (2013). Adapting to climate change: The remarkable decline in the U.S. temperature-mortality relationship over the 20th century. *Journal of Political Economy*, 124(1). <https://doi.org/10.3386/w18692>
8. Hibbard, K.A., F.M. Hoffman, D. Huntzinger, and T.O. West, 2017: Changes in land cover and terrestrial biogeochemistry. In: Climate Science Special Report: Fourth National Climate Assessment, Volume I [Wuebbles, D.J., D.W. Fahey, K.A. Hibbard, D.J. Dokken, B.C. Stewart, and T.K. Maycock (eds.)]. U.S. Global Change Research Program, Washington, DC, USA, pp. 277-302, doi: 10.7930/J0416V6X.
9. Environmental Protection Agency. (2023, August 28). *Heat Island Impacts*. EPA. <https://www.epa.gov/heatislands/heat-island-impacts>
10. *Urban population*. World Bank Open Data. (n.d.). <https://data.worldbank.org/indicator/SP.URB.TOTL?view=map>
11. *Urban Development*. World Bank. (2023, April 3). <https://www.worldbank.org/en/topic/urbandevelopment/overview>
12. Gamble, J. L., Hurley, B. J., Schultz, P. A., Jaglom, W. S., Krishnan, N., & Harris, M. (2013). Climate change and older Americans: State of the science. *Environmental Health Perspectives*, 121(1), 15–22. <https://doi.org/10.1289/ehp.120522310>.

13. Hansen, A., Bi, L., Saniotis, A., & Nitschke, M. (2013). Vulnerability to extreme heat and climate change: Is ethnicity a factor? *Global Health Action*, 6(1), 21364. <https://doi.org/10.3402/gha.v6i0.21364>
14. Egede, L. E., Walker, R. J., Campbell, J. A., Linde, S., Hawks, L. C., & Burgess, K. M. (2023). Modern day consequences of historic redlining: Finding a path forward. *Journal of General Internal Medicine*, 38(6), 1534–1537. <https://doi.org/10.1007/s11606-023-08051-4>
15. Tamme Carleton, Amir Jina, Michael Delgado, Michael Greenstone, Trevor Houser, Solomon Hsiang, Andrew Hultgren, Robert E Kopp, Kelly E McCusker, Ishan Nath, James Rising, Ashwin Rode, Hee Kwon Seo, Arvid Viaene, Jiakan Yuan, Alice Tianbo Zhang, Valuing the Global Mortality Consequences of Climate Change Accounting for Adaptation Costs and Benefits, *The Quarterly Journal of Economics*, Volume 137, Issue 4, November 2022, Pages 2037–2105, <https://doi.org/10.1093/qje/qjac020>
16. Vicedo-Cabrera, A. M., Scovronick, N., Sera, F., Royé, D., Schneider, R., Tobias, A., Astrom, C., Guo, Y., Honda, Y., Hondula, D. M., Abrutzky, R., Tong, S., Coelho, M. de, Saldiva, P. H., Lavigne, E., Correa, P. M., Ortega, N. V., Kan, H., Osorio, S., ... Gasparrini, A. (2021). The burden of heat-related mortality attributable to recent human-induced climate change. *Nature Climate Change*, 11(6), 492–500. <https://doi.org/10.1038/s41558-021-01058-x>
17. Gasparrini, A., Guo, Y., Hashizume, M., Lavigne, E., Zanobetti, A., Schwartz, J., Tobias, A., Tong, S., Rocklöv, J., Forsberg, B., Leone, M., De Sario, M., Bell, M. L., Guo, Y.-L. L., Wu, C., Kan, H., Yi, S.-M., de Sousa Zanotti Staglorio Coelho, M., Saldiva, P. H., ... Armstrong, B. (2015). Mortality risk attributable to high and low ambient temperature: A multicountry observational study. *The Lancet*, 386(9991), 369–375. [https://doi.org/10.1016/s0140-6736\(14\)62114-0](https://doi.org/10.1016/s0140-6736(14)62114-0)
18. Yuan, L., Madaniyazi, L., Vicedo-Cabrera, A. M., Honda, Y., Ng, C. F., Ueda, K., Oka, K., Tobias, A., & Hashizume, M. (2023). A nationwide comparative analysis of temperature-related mortality and morbidity in Japan. *Environmental Health Perspectives*, 131(12). <https://doi.org/10.1289/ehp12854>
19. Gould, C., Heft-Neal, S., Heaney, A., Bendavid, E., Callahan, C., Kiang, M., Zivin, J. S., & Burke, M. (2024). *Temperature Extremes Impact Mortality and Morbidity Differently*. <https://doi.org/10.3386/w32195>
20. Green, H., Bailey, J., Schwarz, L., Vanos, J., Ebi, K., & Benmarhnia, T. (2019). Impact of heat on mortality and morbidity in low and middle income countries: A review of the epidemiological evidence and considerations for future research. *Environmental Research*, 171, 80–91. <https://doi.org/10.1016/j.envres.2019.01.010>
14. *Mortality data - vital statistics NCHS MULTIPLE CAUSE OF DEATH DATA*. NBER. (n.d.). <https://www.nber.org/research/data/mortality-data-vital-statistics-nchs-multiple-cause-death-data>
21. Zhang, T., Zhou, Y., Zhao, K., Zhu, Z., Chen, G., Hu, J., & Wang, L. (2022). A global dataset of daily maximum and minimum near-surface air temperature at 1 km resolution over land (2003–2020). *Earth System Science Data*, 14(12), 5637–5649. <https://doi.org/10.5194/essd-14-5637-2022> 15. NASA. (n.d.-a). *Welcome to ECOSTRESS - ECOSTRESS*. NASA. <https://ecostress.jpl.nasa.gov/>

22. *Technical documentation: Heat waves.* EPA. (2021, April).  
[https://www.epa.gov/sites/default/files/2021-04/documents/heat-waves\\_td.pdf](https://www.epa.gov/sites/default/files/2021-04/documents/heat-waves_td.pdf)

23. Emily A. Shrider And John Creamer. (2023, September 12). *Poverty in the United States: 2022.* Census.gov. <https://www.census.gov/library/publications/2023/demo/p60-280.html>

24. *Overpayment and overcrowding.* California Department of Housing and Community Development. (n.d.).  
<https://www.hcd.ca.gov/planning-and-community-development/housing-elements/building-blocks/overpayment-payment-and-overcrowding>

25. *Hospital emergency department - characteristics by Facility (Pivot Profile) - dataset - california health and human services open data portal.* California Department of Public Health. (n.d.).  
<https://data.chhs.ca.gov/dataset/hospital-emergency-department-characteristics-by-facility-pivot-profile>

26. *Death profiles by ZIP code - dataset - california health and human services open data portal.* California Department of Public Health. (n.d.-a).  
<https://data.chhs.ca.gov/dataset/death-profiles-by-zip-code>

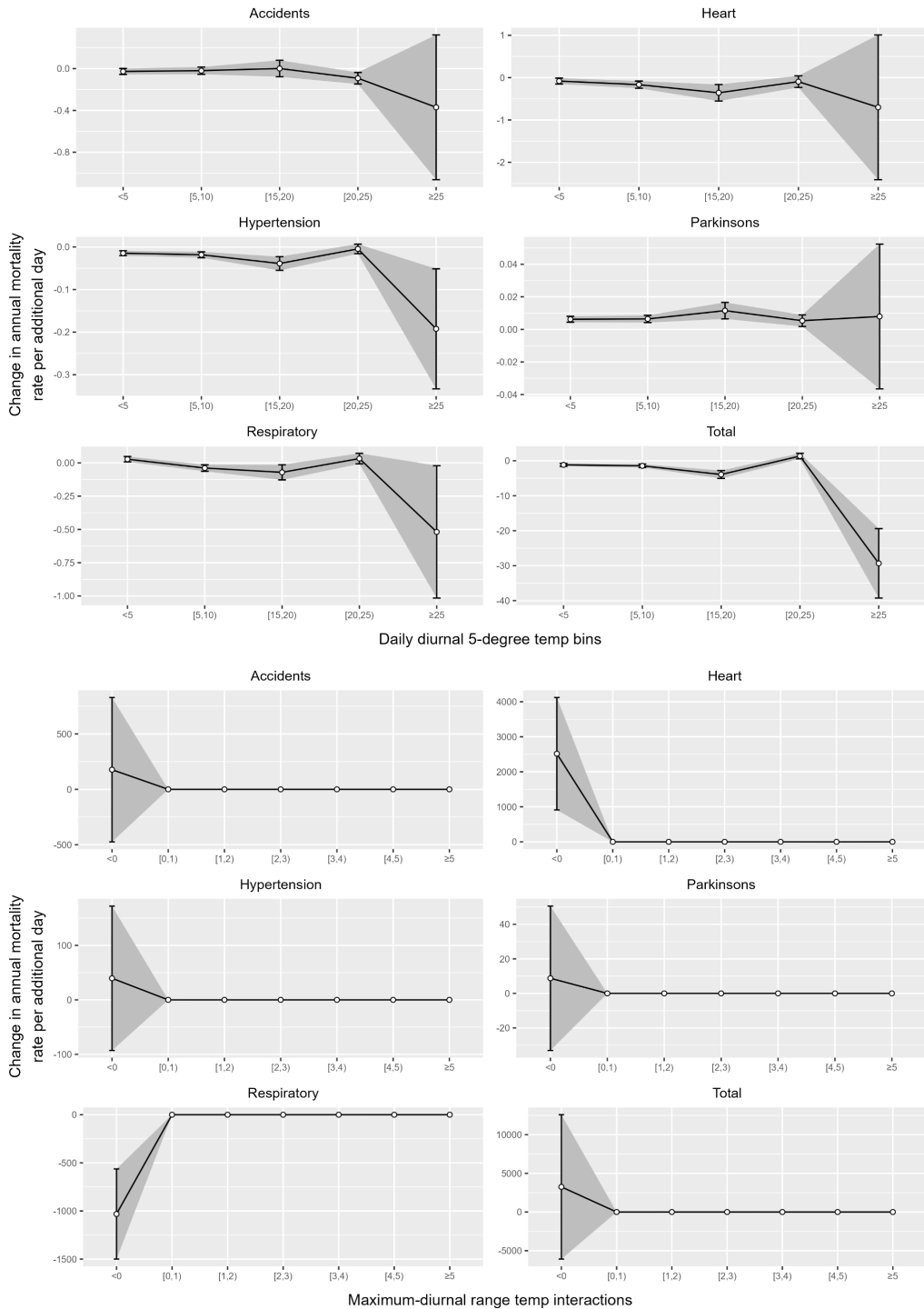
27. Shreevastava, A., Hulley, G. C., Prasanth, S., Yin, Y., Chakraborty, T., Ramos Aguilera, D., Peplinski, M., & Sanders, K. (2023). *Unequal heat exposure in urban areas: Unraveling the role of historic redlining and present-day inequities in Los Angeles.* NASA/ADS.  
<https://ui.adsabs.harvard.edu/abs/2023AGUFMSY12A..07S/abstract>

## VI. Acknowledgments

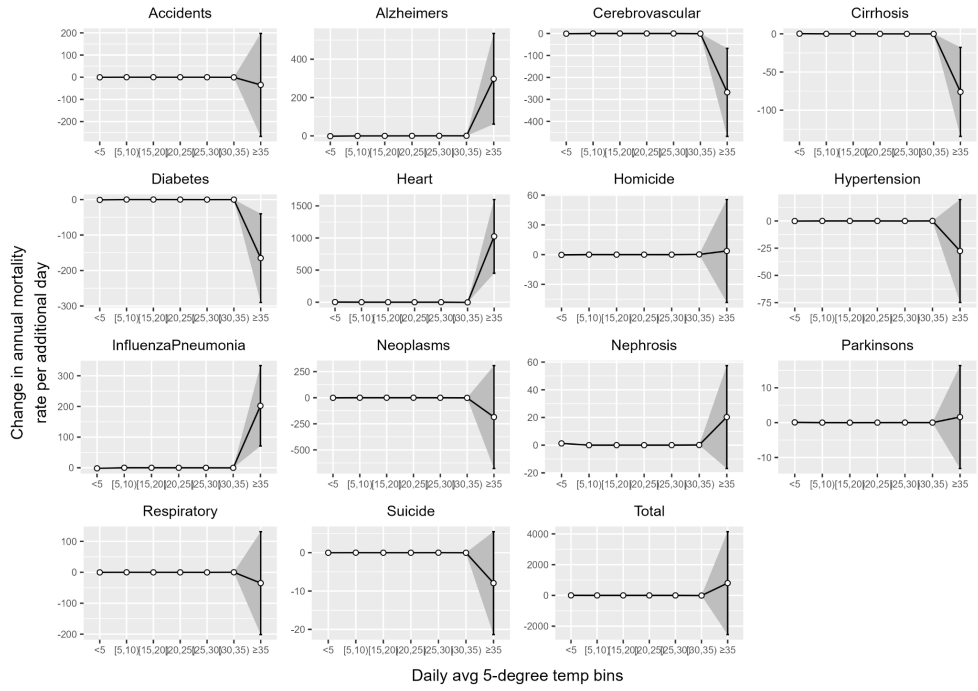
I'd like to thank Prof. Hannah Druckenmiller for her support, guidance, and mentorship throughout the summer. Thank you to Dr. Anamika Shreevastava and Diego Ramos Aguilera for their assistance and guidance throughout the research journey and with understanding the PCA. Thank you Dr. and Mrs. Harris for generously supporting this project in memory of Dr. James J. Morgan.

## VII. Appendices

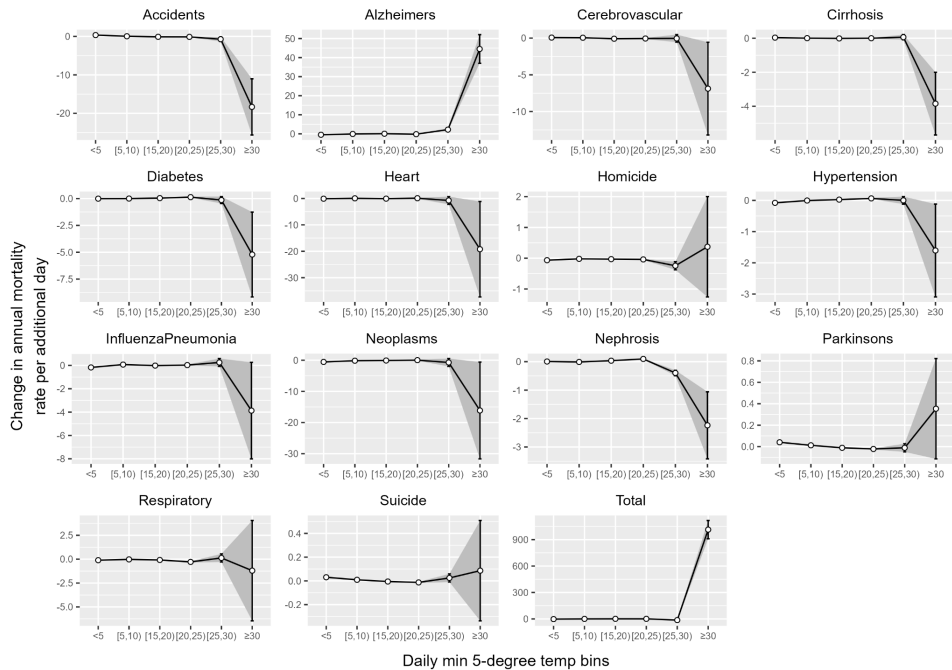
### Cause-specific mortality



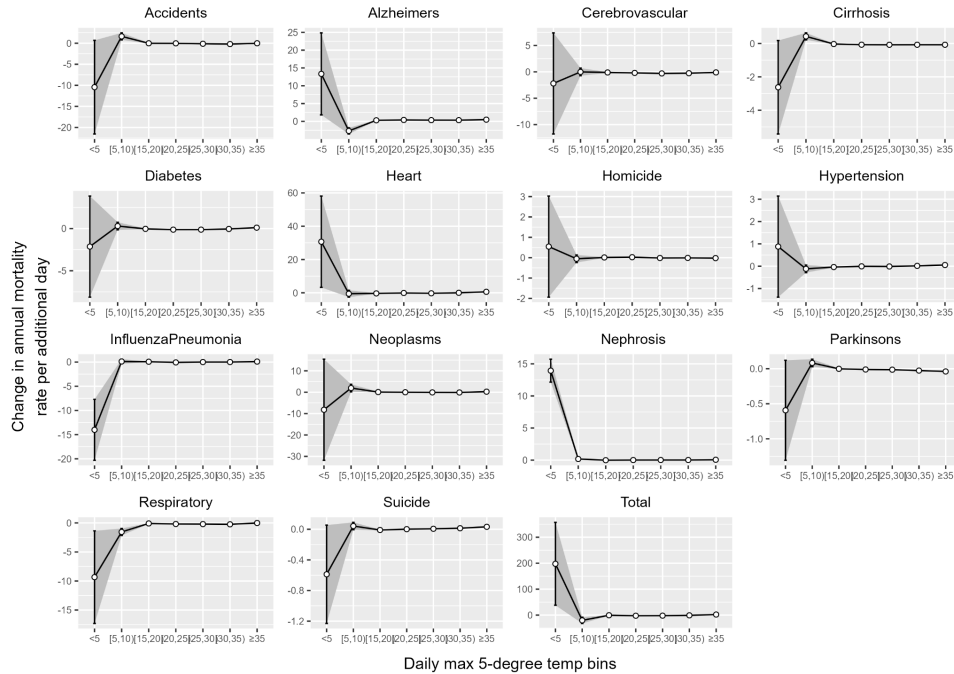
**Figure 13** Selected cause-specific mortality estimates for diurnal range and maximum-diurnal range temperatures.



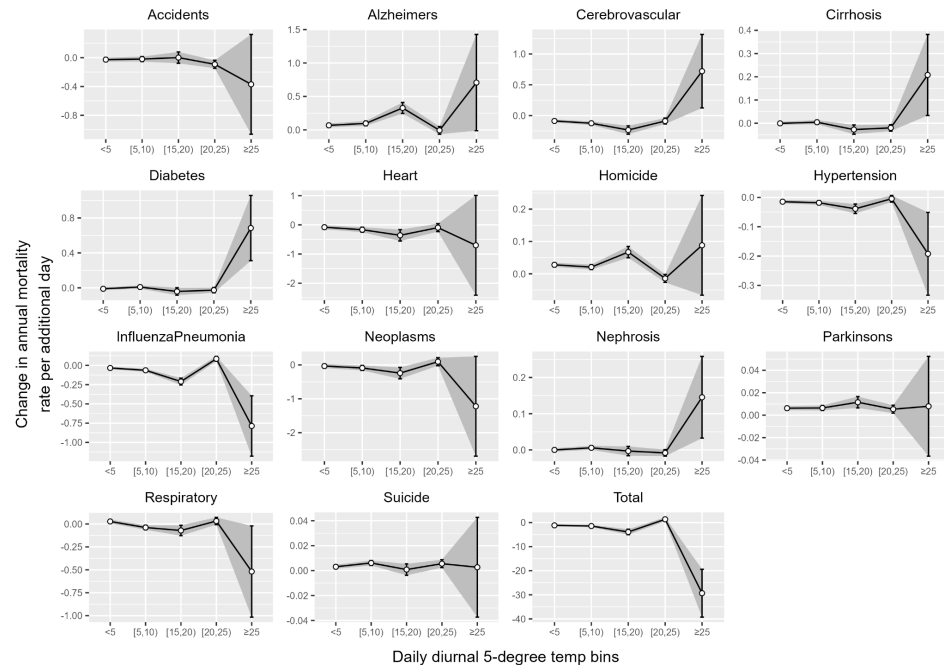
**Figure 14** Cause-specific mortality estimates regressed on average temperature bins. All causes from the health dataset are included.



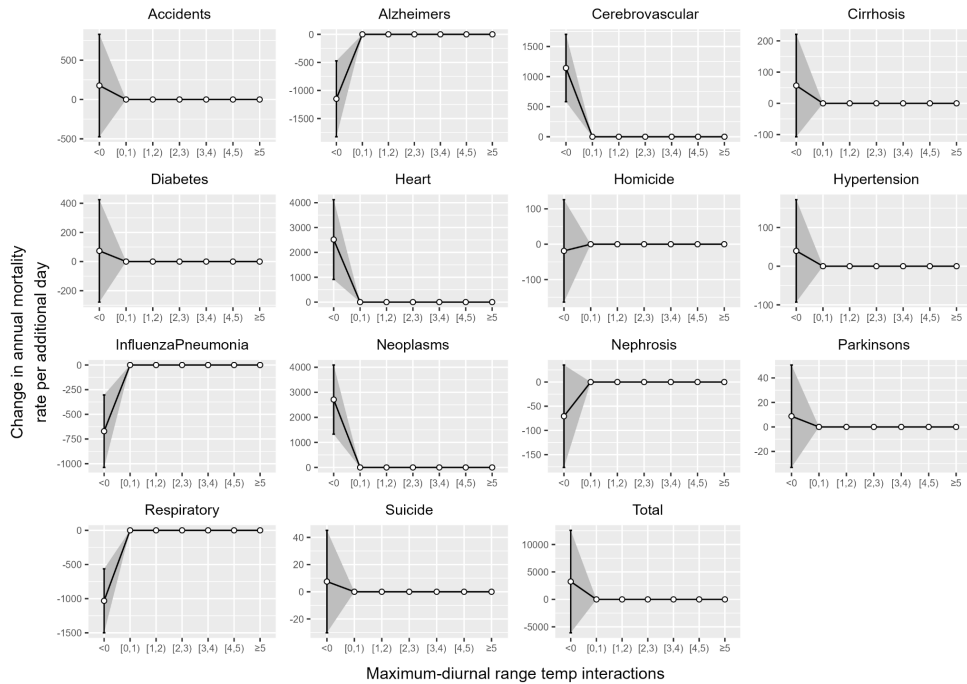
**Figure 15** Cause-specific mortality estimates regressed on minimum temperature bins. All causes from the health dataset are included.



**Figure 16** Cause-specific mortality estimates regressed on maximum temperature bins. All causes from the health dataset are included.

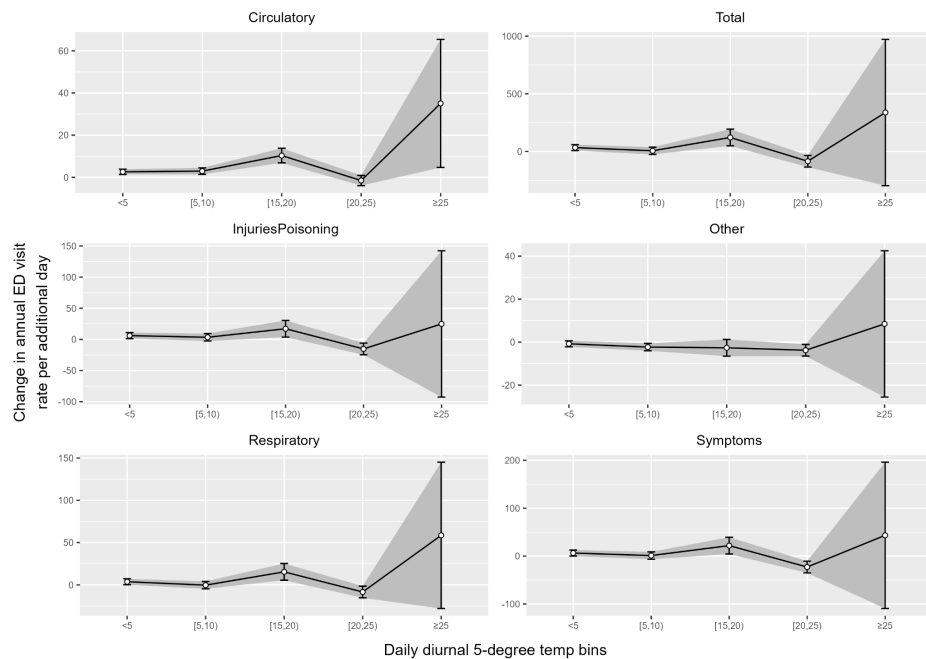


**Figure 17** Cause-specific mortality estimates regressed on diurnal range temperature bins. All causes from the health dataset are included.



**Figure 18** Cause-specific mortality estimates regressed on maximum-diurnal range temperature bins. All causes from the health dataset are included.

### Cause-specific morbidity



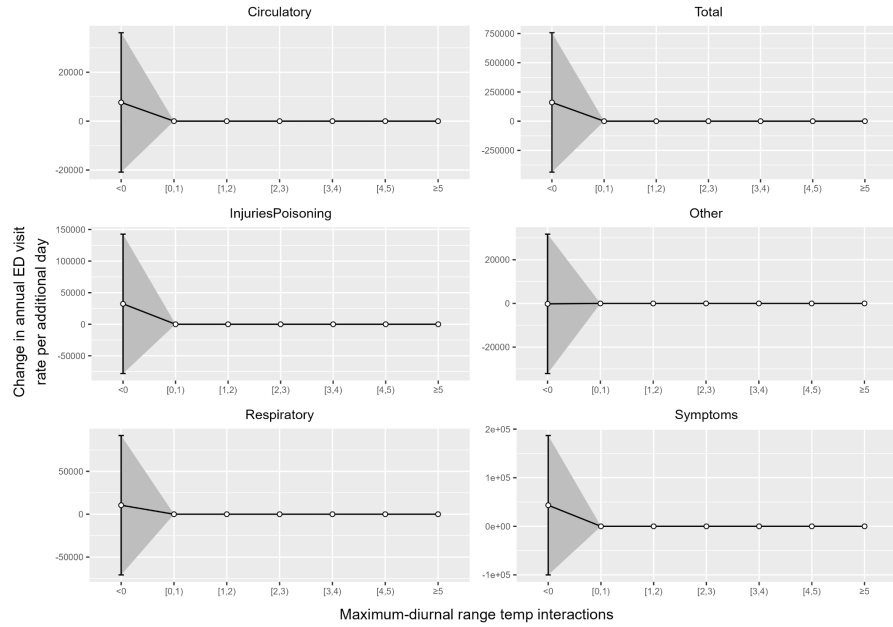


**Figure 19** Selected cause-specific morbidity estimates regressed on diurnal and maximum-diurnal range temperature bins.

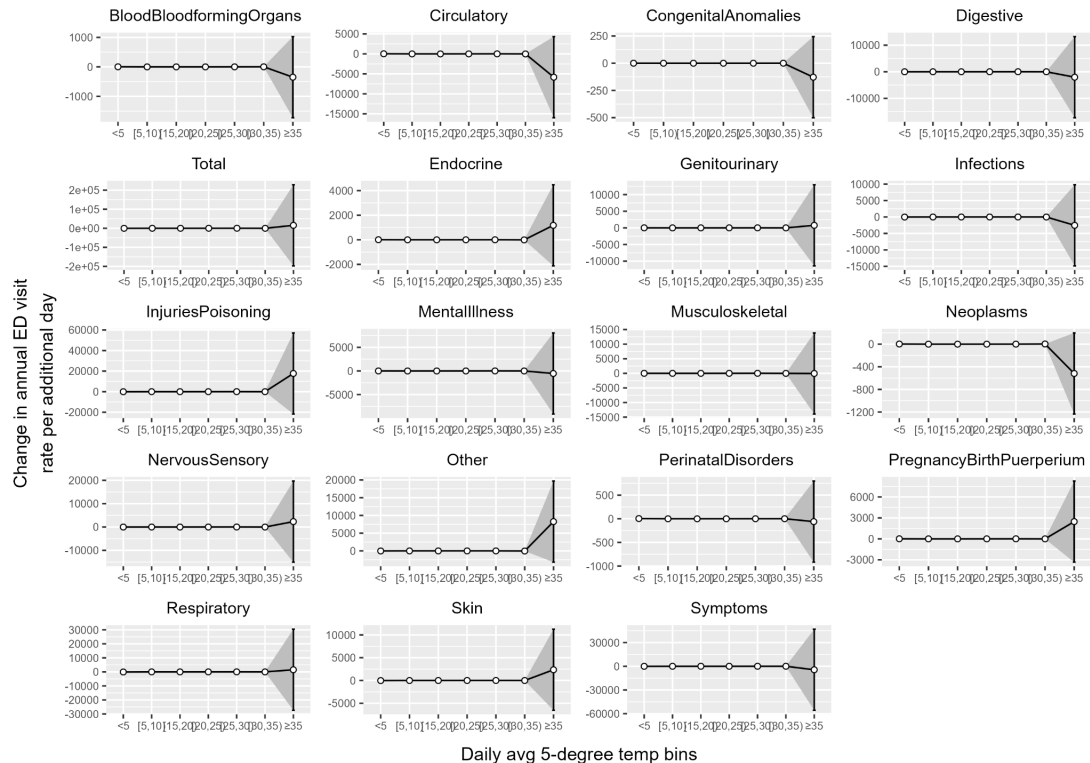


**Figure 20** Cause-specific morbidity estimates regressed on average temperature bins. All causes from the health dataset are included.

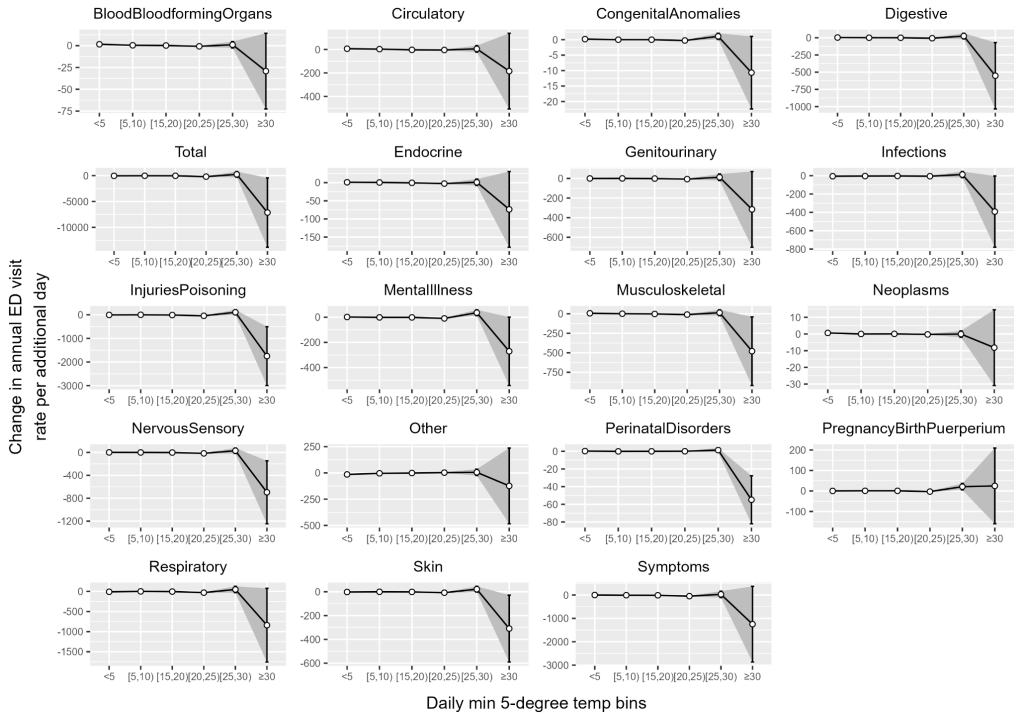


**Figure 21** Cause-specific morbidity estimates regressed on minimum temperature bins. All causes from the health dataset are included.

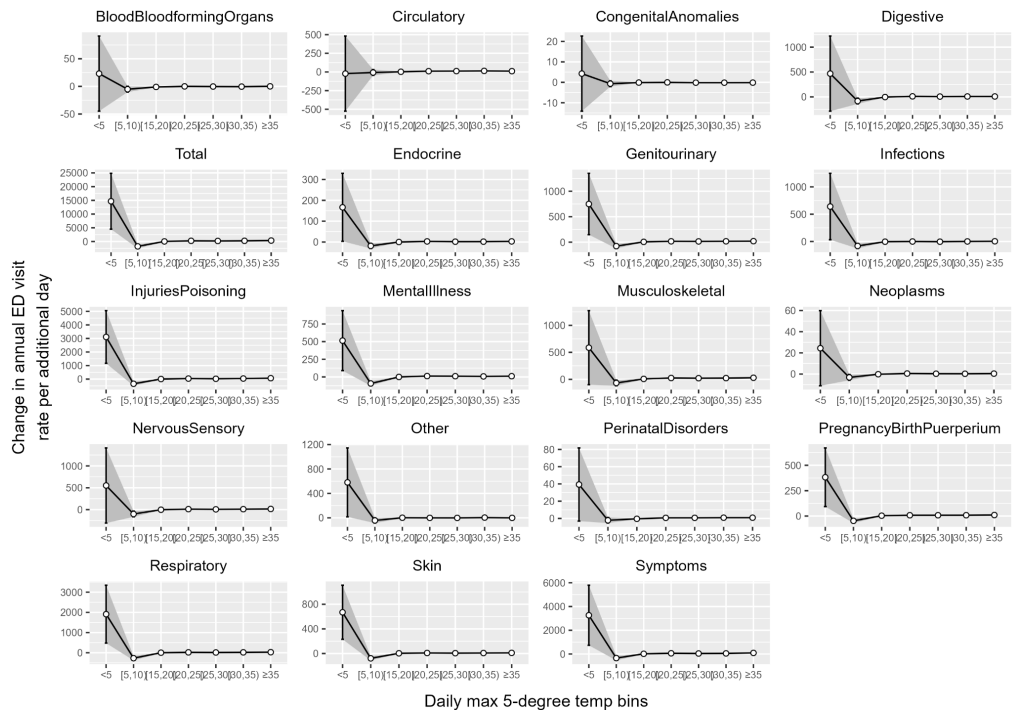


**Figure 22** Cause-specific morbidity estimates regressed on maximum temperature bins. All causes from the health dataset are included.

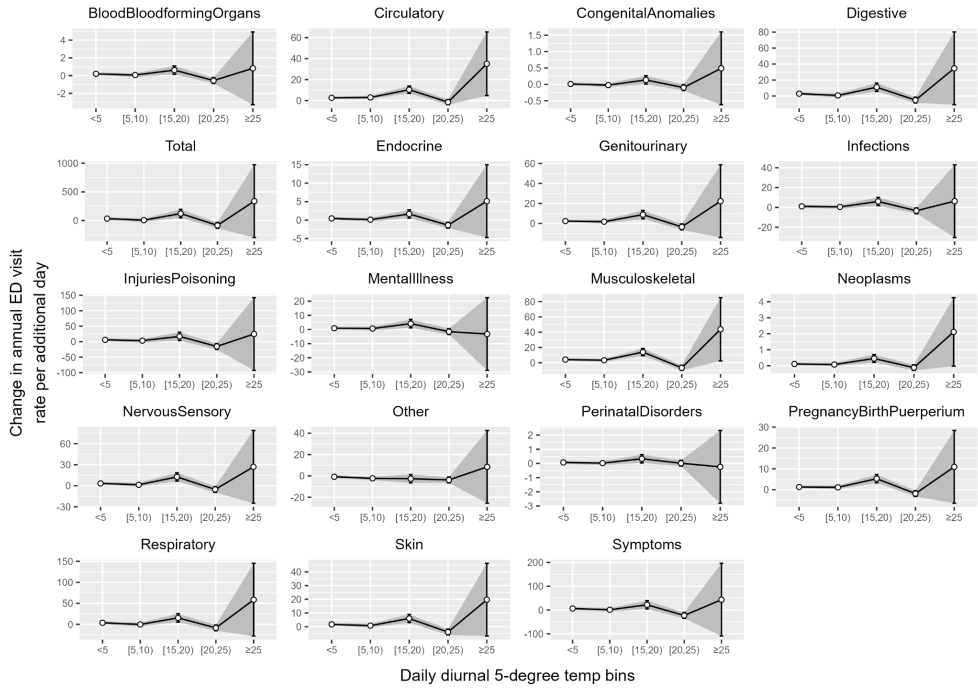


**Figure 23** Cause-specific morbidity estimates regressed on diurnal range temperature bins. All causes from the health dataset are included.

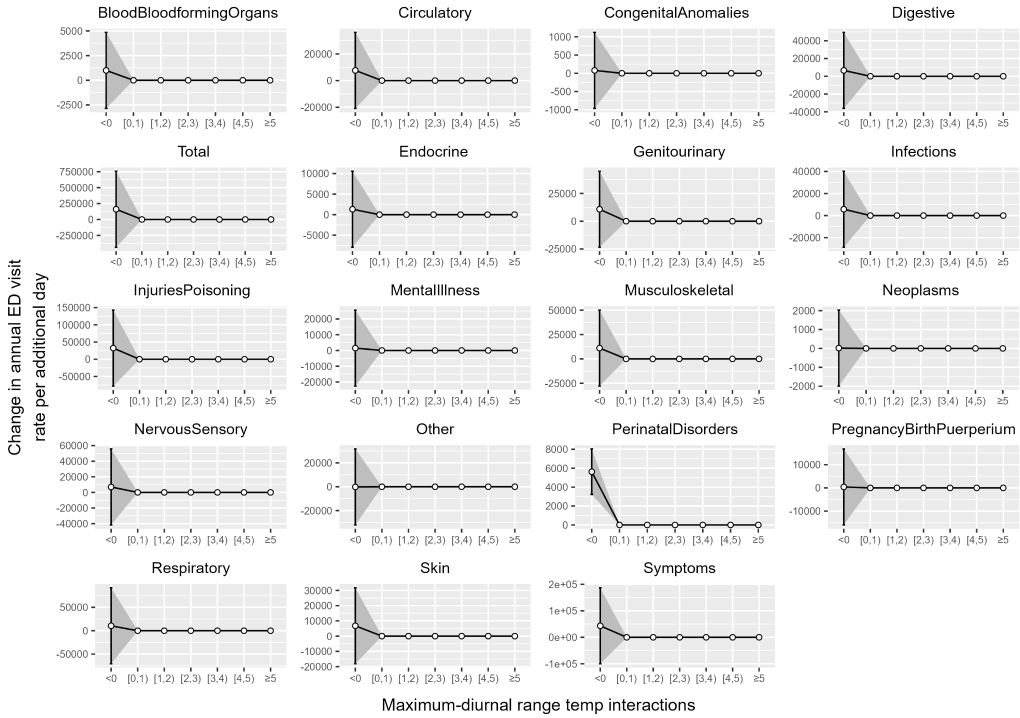


**Figure 23** Cause-specific morbidity estimates regressed on maximum-diurnal range temperature bins. All causes from the health dataset are included.

## Heatwave mortality

Variable	Coefficient	Standard error	P-value
< 5	5.157	13.432	0.701
[5, 10)	0.438	0.702	0.533
[15, 20)	0.232	0.291	0.426
[20, 25)	0.824	0.527	0.118
[25, 30)	-0.089	0.827	0.914
[30, 35)	-8.823	5.099	0.084
≥ 35	997.949	3333.376	0.765
Heatwave	-77.808	19.363	0
Heatwave <sup>2</sup>	14.971	3.176	0
Heatwave <sup>3</sup>	-0.822	0.162	0

**Table 4** Mortality rates regressed on average temperature bins and heatwave counts. Heatwave coefficients show a negative cubic relationship consistent with the mortality-heatwave model in Table 2. The [10, 15) bin is omitted as the reference bin.

Variable	Coefficient	Standard error	P-value
< 5	-1.151	1.63	0.48
[5, 10)	0.481	0.67	0.473
[15, 20)	1.574	0.642	0.014
[20, 25)	1.457	1.27	0.252
[25, 30)	-14.491	8.391	0.084
≥ 30	993.218	103.742	0
Heatwave	-84.459	19.159	0
Heatwave <sup>2</sup>	14.881	3.182	0

Heatwave <sup>3</sup>	-0.777	0.162	0
-----------------------	--------	-------	---

**Table 5** Mortality rates regressed on minimum temperature bins and heatwave counts. Heatwave coefficients show a negative cubic relationship consistent with the mortality-heatwave model in Table 2. The [10, 15) bin is omitted as the reference bin.

Variable	Coefficient	Standard error	P-value
< 5	172.608	159.239	0.278
[5, 10)	-17.543	11.92	0.141
[15, 20)	-0.41	1.329	0.758
[20, 25)	-2.487	1.377	0.071
[25, 30)	-1.656	1.547	0.284
[30, 35)	-0.778	1.728	0.653
≥ 35	1.889	2.215	0.394
Heatwave	-79.365	18.887	0
Heatwave <sup>2</sup>	14.37	3.17	0
Heatwave <sup>3</sup>	-0.774	0.162	0

**Table 6** Mortality rates regressed on maximum temperature bins and heatwave counts. Heatwave coefficients show a negative cubic relationship consistent with the mortality-heatwave model in Table 2. The [10, 15) bin is omitted as the reference bin.

Variable	Coefficient	Standard error	P-value
< 5	-1.14	0.407	0.005
[5, 10)	-1.451	0.499	0.004
[15, 20)	-3.962	1.136	0
[20, 25)	1.297	0.79	0.101

$\geq 25$	-30.22	9.906	0.002
Heatwave	-80.186	18.386	0
Heatwave <sup>2</sup>	14.846	3.076	0
Heatwave <sup>3</sup>	-0.806	0.158	0

**Table 7** Mortality rates regressed on diurnal range temperature bins and heatwave counts. Heatwave coefficients show a negative cubic relationship consistent with the mortality-heatwave model in Table 2. The [10, 15) bin is omitted as the reference bin.

Variable	Coefficient	Standard error	P-value
< 0	-128.882	856.138	0.88
[0, 1)	17.352	44.743	0.698
[1, 2)	-35.268	18.528	0.057
[3, 4)	37.596	33.601	0.263
[4, 5)	189.245	52.739	0
$\geq 5$	13958.102	212463.601	0.948
Heatwave	637.902	1234.137	0.605
Heatwave <sup>2</sup>	-171.262	202.45	0.398
Heatwave <sup>3</sup>	6.642	10.333	0.52

**Table 8** Mortality rates regressed on maximum-diurnal range temperature bins and heatwave counts. Heatwave coefficients show a positive cubic relationship consistent with the morbidity-heatwave model in Table 3. The [2, 3) is omitted as the reference bin.

### Heatwave morbidity

Variable	Coefficient	Standard error	P-value
< 5	-128.882	856.138	0.88

[5, 10)	17.352	44.743	0.698
[15, 20)	-35.268	18.528	0.057
[20, 25)	37.596	33.601	0.263
[25, 30)	189.245	52.739	0
[30, 35)	-69.186	325.022	0.831
$\geq 35$	13958.102	212463.601	0.948
Heatwave	637.902	1234.137	0.605
Heatwave <sup>2</sup>	-171.262	202.45	0.398
Heatwave <sup>3</sup>	6.642	10.333	0.52

**Table 9** Morbidity rates regressed on average temperature bins and heatwave counts. Heatwave coefficients show a positive cubic relationship consistent with the morbidity-heatwave model in Table 3. The [10, 15) bin is omitted as the reference bin.

Variable	Coefficient	Standard error	P-value
< 5	-68.797	105.409	0.514
[5, 10)	-47.802	43.368	0.27
[15, 20)	-45.211	41.526	0.276
[20, 25)	-198.06	82.174	0.016
[25, 30)	286.49	542.751	0.598
$\geq 30$	-6700.16	6710.13	0.318
Heatwave	2657.973	1239.195	0.032
Heatwave <sup>2</sup>	-451.773	205.786	0.028
Heatwave <sup>3</sup>	20.111	10.461	0.055

**Table 10** Morbidity rates regressed on minimum temperature bins and heatwave counts. Heatwave coefficients show a positive cubic relationship consistent with the morbidity-heatwave model in Table 3. The [10, 15) bin is omitted as the reference bin.

Variable	Coefficient	Standard error	P-value
< 5	15552.716	10164.744	0.126
[5, 10)	-1759.621	760.865	0.021
[15, 20)	18.127	84.836	0.831
[20, 25)	241.544	87.889	0.006
[25, 30)	165.615	98.731	0.094
[30, 35)	241.054	110.289	0.029
≥ 35	367.792	141.373	0.009
Heatwave	3009.324	1205.642	0.013
Heatwave <sup>2</sup>	-508.942	202.333	0.012
Heatwave <sup>3</sup>	22.83	10.316	0.027

**Table 11** Morbidity rates regressed on maximum temperature bins and heatwave counts. Heatwave coefficients show a positive cubic relationship consistent with the morbidity-heatwave model in Table 3. The [10, 15) bin is omitted as the reference bin.

Variable	Coefficient	Standard error	P-value
< 5	33.096	26.054	0.204
[5, 10)	2.335	31.969	0.942
[15, 20)	108.479	72.698	0.136
[20, 25)	-83.055	50.589	0.101
≥ 25	359.943	634.009	0.57

Heatwave	2234.693	1176.751	0.058
Heatwave <sup>2</sup>	-370.213	196.882	0.06
Heatwave <sup>3</sup>	15.713	10.09	0.119

**Table 12** Morbidity rates regressed on diurnal range temperature bins and heatwave counts. Heatwave coefficients show a positive cubic relationship consistent with the morbidity-heatwave model in Table 3. The [10, 15) bin is omitted as the reference bin.

Variable	Coefficient	Standard error	P-value
< 0	205478.366	596212.82	0.73
[0, 1)	-19.967	40.635	0.623
[1, 2)	1.464	8.465	0.863
[3, 4)	-2.637	14.24	0.853
[4, 5)	-14.299	25.889	0.581
≥ 5	4.529	15.863	0.775
Heatwave	2430.502	1188.518	0.041
Heatwave <sup>2</sup>	-399.032	198.743	0.045
Heatwave <sup>3</sup>	17.129	10.206	0.093

**Table 13** Morbidity rates regressed on maximum-diurnal range temperature bins and heatwave counts. Heatwave coefficients show a positive cubic relationship consistent with the morbidity-heatwave model in Table 3. The [2, 3) bin is omitted as the reference bin.